JRC Scientific and Technical Reports

Near-Coastal Features of the NW Mediterranean Sea

Space and time heterogeneity of atmospheric forcing, vertical mixing and algal blooming, from satellite observations and model simulations (1997-2007)

V. Barale, E. Garcia Gorriz, N. Hoepffner, A. Stips

EUR 23708 EN - 2008

JRC EUROPEAN COMMISSION

Institute for Environment and Sustainability

The mission of the Institute for Environment and Sustainability is to provide scientific and technical support to the European Union's policies for protecting the environment and the EU Strategy for Sustainable Development.

European Commission
Directorate-General Joint Research Centre
Institute for Environment and Sustainability

Contact information
Address: V. Barale, European Commission, Joint Research Centre, Institute for Environment and Sustainability, Via E. Fermi 2749 (tp 272), I-21027 Ispra (VA), Italy
E-mail: vittorio.barale@jrc.ec.europa.eu
Tel.: +39 0332 789274
Fax: +39 0332 789034

http://ies.jrc.ec.europa.eu
http://www.jrc.ec.europa.eu

JRC 49504

EUR 23708 EN

ISSN 1018-5593

Luxembourg: Office for Official Publications of the European Communities

Printed in Italy

Title

Near-Coastal Features of the NW Mediterranean Sea
Space and time heterogeneity of atmospheric forcing, vertical mixing and algal blooming, from satellite observations and model simulations (1997-2007)

Authors

Vittorio Barale
Elisa Garcia Gorriz
Nicolas Hoepffner
Adolf Stips

European Commission, Joint Research Centre
Institute for Environment and Sustainability
Global Environment Monitoring Unit
Via E. Fermi 2749 (tp 272), I-21027 Ispra (VA), Italy

e-mail	tel	fax
vittorio.barale@jrc.ec.europa.eu	+39 0332 789274	+39 0332 789034
elisa.garcia-gorriz@jrc.ec.europa.eu	+39 0332 786268	+39 0332 789034
nicolas.hoepffner@jrc.ec.europa.eu	+39 0332 789873	+39 0332 789034
adolf.stips@jrc.ec.europa.eu	+39 0332 789876	+39 0332 789034

Abstract

Data derived from satellite observations and model simulations were used to assess space–time heterogeneity of atmospheric forcing, vertical mixing and algal blooming of the Ligurian-Provençal Sea, in the north-western Mediterranean basin. The ecosystem response to changing seasonal conditions in the Gulf of Lion (40.5–42.5°N, 3.5–7.5°E) was examined over 10 consecutive annual cycles (Sep 1997 – Aug 2007). In this environmental hotspot, atmospheric forcing causes deep convective processes and consequent nutrient upwelling in the water column. As phytoplankton growth in the otherwise oligotrophic basin is always nutrient-limited, the blooming triggered by these processes reflects the prevailing wind field patterns.

Acknowledgements

The exploratory research described in the present report has been undertaken as part of the Framework Programme 7 (FP7) Action 21203 PROCAS. The images and data used in this report were acquired in part using the Environmental Marine Information System (EMIS), of the EC Joint Research Centre (JRC), Institute for Environment and Sustainability (IES), and in part using the GES-DISC Interactive Online Visualization ANd aNalysis Infrastructure (Giovanni), of the NASA Goddard Earth Sciences (GES), Data and Information Services Center (DISC).

Reference

V. Barale, E. Garcia Gorriz, N. Hoepffner, A. Stips (2008). Near- Coastal Features of the NW Mediterranean Sea. Space and time heterogeneity of atmospheric forcing, vertical mixing and algal blooming, from satellite observations and model simulations (1997-2007). European Commission, EUR 23708 EN, pp. 60.

Table of Contents

1. Introduction 7
1.1 Main Environmental Traits of the Mediterranean Basin 8
1.2 The Gulf of Lion in the Ligurian-Provençal Sea 9
Plate 1. Mediterranean Sea, map and nomenclature 11
Plate 2. Conceptual annual cycles of phytoplankton biomass . . 12
Plate 3. Seasonality of the Ligurian-Provençal Sea 13
Plate 4. The Gulf of Lion environmental hotspot 14

2. Data Sources 15
2.1 Chlorophyll-like pigment concentration (*Chl*) Data Sets 15
2.2 Sea Surface Temperature (*SST*) Sample Data 17
2.3 Wind Speed (*WS*) and Direction Data 17
2.4 Model-derived Data 18
Plate 5. JRC vs NASA SeaWiFS Chl estimates, time series 20
Plate 6. JRC vs NASA SeaWiFS Chl estimates, correlation 21

3. The SeaWiFS *Chl* historical time series 23
3.1 Time series of *Chl* monthly averages 23
3.2 Long-term trend: the historical CZCS record 24
Plate 7. Mediterranean Sea, SeaWiFS Chl annual climatology . 26
Plate 8. Gulf of Lion, SeaWiFS Chl monthly climatology 27
Plate 9. Gulf of Lion, area of interest for statistical analysis . . 28
Plate 10. Chl area-averaged values, inter-annual variability . . 29
Plate 11. Chl area-averaged values, inter-annual trends 30
Plate 12. Chl and WS area-averaged climatological values . . . 31
Plate 13. Mediterranean Sea, CZCS Chl monthly climatology . . 32

4. Algal blooms, surface temperatures and wind patterns 33
Plate 14. Monthly mean WS (Jan-May) in the Gulf of Lion . . . 35
Plate 15. Monthly mean Chl (Jan-May) in the Gulf of Lion . . . 36
Plate 16. Chl and WS 2000-2007 time series & climatology . . . 37
Plate 17. Chl and WS 2000-2007 regression analysis (1) 38
Plate 18. Chl and WS 2000-2007 regression analysis (2) 39

5. Comparison of satellite data and model results 41
Plate 19. Gulf of Lion, climatological mixed layer temperature . 43
Plate 20. Gulf of Lion, climatological mixed layer depth 44
Plate 21. SST, m. l. temperature & depth (series) 45
Plate 22. SST, m. l. temperature & depth (regression) 46
Plate 23. Chl, SST, m. l. temperature & depth (series) 47
Plate 24. Chl, SST, m. l. temperature & depth (regression) . . . 48
Plate 25. Chl & mixed layer depth correlation 49

6. Conclusion 51

References 53

1. Introduction

The north-western area of the Mediterranean Sea can be classified as one of the most intriguing environmental hotspots of the marginal and enclosed basins surrounding the European continent. In the same region, unique physical processes such as strong air-sea interactions and bottom water formation are coupled to the most intense primary (and secondary) production of the entire basin, and a resulting trophic chain culminating with a sizeable resident population of fin whales (*Balaenoptera physalus*). This has led to the establishment, in 1999, of one of the first, and largest, pelagic protected areas in the world – the *Pelagos* International Sanctuary for Marine Mammals (Notarbartolo di Sciara *et al.*, 2008) – the requirements of which have to coexist with a score of human activities, ranging from intense shipping through some of the major southern European ports, to offshore oil extraction along the Catalan coast and to prime touristic destinations such as the *Côte d'Azur* and the *Riviera*. Assessing the relationship between ecological dynamics and related forcing functions, in such a peculiar hotspot, demands for novel, specific capabilities for environmental monitoring. The broad range of natural processes occurring at the hotspot, and the wide span of space and time scales to be covered, requires that suitable surveillance tools and methods be evaluated and then applied systematically, over large areas and for long periods. Of course, the collection of data from traditional surface platforms remains a key component of most environmental assessments, in this as in most other marine regions. However, it is the combination of remote sensing and ecological modelling that has provided, in recent years, an increasing degree of success in addressing this issue.

A comparison of satellite data and concurrent model simulations was used, in the present case, to explore the coupling between algal blooming and atmospheric forcing in the north-western Mediterranean Sea, and in the near-coastal region of the Ligurian-Provençal Sea in particular (Plate 1). In this site, conventionally centered at 5°E, 42°N, *i.e.* in the Gulf of Lion, deep convection takes place in winter, due to the effect of northerly winds and negative heat fluxes, which increase the density of surface waters (see *e.g.* Hermann *et al.*, 2008, and references therein). The ensuing vertical mixing brings deep nutrient-rich waters to the surface and then, when the water column stabilizes, favours the onset of sizeable spring blooms (Backhaus *et al.*, 1999). Although highly dynamic, and unstable, these features recur systematically in the area, and are readily observed into optical, thermal and structural data collected from satellite (Barale, 2003).

In the present report, after a brief introduction of the main environmental traits of the Mediterranean basin, and of the peculiarities of the Ligurian-Provençal Sea, the core data sets and model simulations used will be presented. Further, the comparison between algal blooms, wind patterns and model results will be

discussed in detail. Indicators of ecological dynamics – *i.e.* chlorophyll-like pigment concentration, *Chl* hereafter, a marker of phytoplankton biomass – were derived primarily from data collected by the Sea-viewing Wide Field-of-View Sensor (SeaWiFS), which was placed in Earth orbit on the SeaStar satellite in September 1997. The SeaWiFS is a radiometer operating in the visible and near-infrared spectral range, and capable of detecting the subtle variations of ocean colour due to different water constituents (McClain *et al.*, 2004). A qualitative comparison was made with the historical data set collected by the earlier Coastal Zone Color Scanner (CZCS), a similar, if more primitive, visible radiometer which operated between 1978 and 1986 (Hovis et al. 1900). Sample sea surface temperature – *SST* hereafter – data were also considered, as derived from the Along-Track Scanning Radiometer (ATSR, versions 1/2) data set (Murray *et al.*, 1998), and from the Advanced Very High Resolution Radiometer (AVHRR) – a sensor working in the visible and near/thermal infrared spectral range, and operating since the late 1970s' on board various polar orbiting satellites of the NOAA series (Kidwell, 1991) – in the Pathfinder Project version (Kilpatrick *et al.*, 2001). Atmospheric forcing was addressed considering wind speed – *WS* hereafter – derived from the microwave scatterometer SeaWinds, later dubbed QuikScat, which was launched on the QuikBird satellite in June 1999 (Draper and Long, 2002). Finally, the indicators derived from remote sensing data were compared with model data resulting from simulations performed with the General Estuarine Transport Model (GETM), detailed by Burchard and Bolding (2002). The turbulence model used in this study is the 2-equation closure model, based on turbulent kinetic energy and dissipation rate, known as General Ocean Turbulence Model (GOTM). An investigation of this model performance under convective turbulence conditions, which are important for the Gulf of Lion, has been carried out and reported upon by Stips *et al.* (2002).

1.1 Main Environmental Traits of the Mediterranean Basin

Knowledge of the space and time heterogeneity of phytoplankton growth is critical to understand marine ecosystem dynamics (Mann and Lazier, 2006). The seasonal dynamics of phytoplankton biomass in a given basin, at different latitudes, can be described by conceptual models, with a variable degree of complexity (see *e.g.* Yoder and Kennelly 2003 and references therein), but essentially based on a set of simple cases such as those described by Cushing (1959). In this conventional interpretation (see Plate 2), three main situations can be distinguished, on the basis of the key factors limiting phytoplankton growth (*i.e.* the availability of light and nutrients). In a sub-tropical basin, light is available year-round for photosynthetic activities, due to the low latitude; but nutrients, continuously consumed by phytoplankton, are always in short supply. This nutrient limitation is relaxed in winter, when vertical mixing, fostered by more intense atmospheric processes, brings nutrients from deeper waters (where

they constantly accumulate by gravity) to the surface. When the water column stratifies, typically in summer, the phytoplankton runs out of nutrients and photosynthetic activities are reduced to a minimum. In principle, the situation is not different in a sub-polar basin, except that light limitation must be added as well. The enrichment of the surface with nutrients from deep waters still occurs in winter, but there is not enough light available to fuel photosynthesis. Hence, blooming occurs only in spring, when the light increases to acceptable levels. Then, the water column stratifies, nutrients run out and the biomass (also reduced by grazing) drops to a summer minimum. When the stratification breakdown due to cooling temperatures allows again vertical mixing in the water column, providing a new source of nutrients, in fall, a secondary bloom takes place, soon to die off because of the decreasing light level. Finally, in a polar basin, nutrients mixed from deeper waters to the surface by atmospheric forcing are available year-round, but light, due to the high latitude, is available only in summer, when the major blooming occurs.

The Mediterranean Sea is predominantly oligotrophic and appears to behave like a sub-tropical basin, where the light level is never a limiting factor (so that its decrease in winter does not inhibit algal growth), but the nutrient level always is. Thus, blooming occurs primarily in the colder, windy and wet (winter) season, and is due to the biological enrichment of surface waters due to surface cooling, vertical mixing and upwelling, or continental runoff. As atmospheric forcing is not strong enough to drive basin-wide upward transport of nutrient-rich waters from deep layers, winter blooming maintains a patchy character and is mostly limited to those regions where local meteorological conditions, or other factors, drive the nutrient enrichment (Bosc *et al.*, 2004). Conversely, no blooming occurs in the warmer, calm and dry (summer) season, when the water column is strongly stratified and no nutrient supply, from coastal zones or deeper layers, is readily available (Barale, 2005). Due to the climate and circulation of the Mediterranean Sea – a concentration basin that transforms Atlantic water, entering at the surface in the Strait of Gibraltar and flowing eastward, into warmer, saltier Mediterranean water, ultimately sinking and flowing back westward, until exiting at depth in the Strait of Gibraltar – oligotrophy increases from west to east (Barale *et al.*, 2008). Notable exceptions are a few hotspots, corresponding either to sources of continental runoff (often linked to a severe anthropogenic impact) or to regions where atmospheric forcing creates specific local conditions that trigger the sequence of convective processes, nutrient upwelling and algal blooming.

1.2 The Gulf of Lion in the Ligurian-Provençal Sea

The impact of air-sea interactions is particularly evident for the near-coastal area off the Gulf of Lion, in the Ligurian-Provençal Sea (Plate 3) when compared to the remainder of the basin. In this region,

hydrodynamic (and ecological) processes are driven by atmospheric forcing (and, to a lesser extent, by mesoscale circulation and fluvial runoff). The episodic gale-force winds across the Gulf of Lion, *i.e.* the north-westerly Tramontane and the northerly Mistral, cause intense surface cooling and generate transitional circulation patterns (Petrenko *et al.*, 2005). These interact with the main mesoscale circulation feature of the region, *i.e.* the Northern Current, which follows a cyclonic pattern along the continental slope south-east of the Gulf (Millot and Taupier-Letage, 2005). The main freshwater input is due to the Rhône river plume, which is generally advected south-westward by the surface current (Kondrachoff *et al.*, 1994).

The resulting characteristics of surface waters are summarized in Plate 3, where the 1999 series of *SST* and *Chl* maps are presented as monthly means composited from ATSR1/2 and SeaWiFS daily images, respectively. The *SST* maps show where atmospheric forcing in winter (January and February), decreases the temperature and increases the density of surface waters, through strong evaporation and cooling, triggering deep convection processes or even the complete overturning of the water column (Schott *et al.*, 1996). The ensuing vertical mixing ventilates the deepest parts of the basin and brings deep nutrient-rich waters to the surface. The *Chl* maps show that, when the water column stabilizes in spring (March and April), the enrichment of surface waters due to the vertical mixing favours the onset of intense algal blooms, which can continue until summer conditions prevail.

This combination of factors renders the seasonal cycle of the Ligurian-Provençal Sea similar to the sub-polar type seen above, with a production minimum in winter, followed by a spring bloom, another minimum in summer and (occasionally) a secondary fall bloom. However, the winter minimum occurs only in a specific area, the so-called “blue hole” (see *e.g.* the Gulf of Lion in February 2000; Plate 4, left panel) – a notation first introduced by Barale (2000) – and is not due strictly to light limitation, at least in the euphotic zone. In fact, since winter blooming (typical of the sub-tropical case) occurs almost everywhere else, in the north-western Mediterranean, at the same latitude, it is not the lack of sunlight that limits phytoplankton growth. Rather, it is the deep convection, generated by the strong, cold winds directed by the regional orography, that prevents the blooming to occur in this place and season. Phytoplankton are removed from the euphotic zone and advected to great depth (greater than 2000 m, in certain cases), so that they cannot make it back to the surface and photosynthetize again, after being exposed to the pressure and darkness of the deep water column for a prolongued period. It is only when this advection stops, and the water column stabilizes, that the blooming can start, taking advantage of the nutrient enrichment of surface waters due to the prolongued period of vertical mixing (see *e.g.* the Gulf of Lion in April 2000; Plate 4, right panel).

Plate 1. Mediterranean Sea, map and nomenclature

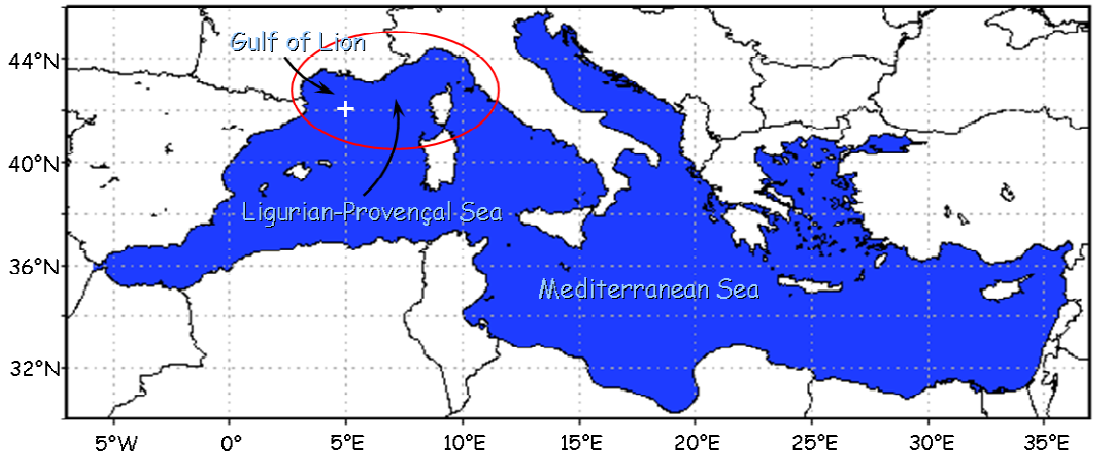

Plate 1. Mediterranean Sea map. The red oval corresponds to the region of the Ligurian-Provençal Sea considered for the present study, which concentrated in particular over the Gulf of Lion area. The site where winter deep convection takes place (conventionally centered at 5°E, 42°N) is represented by the white cross.

Plate 2. Conceptual annual cycles of phytoplankton biomass

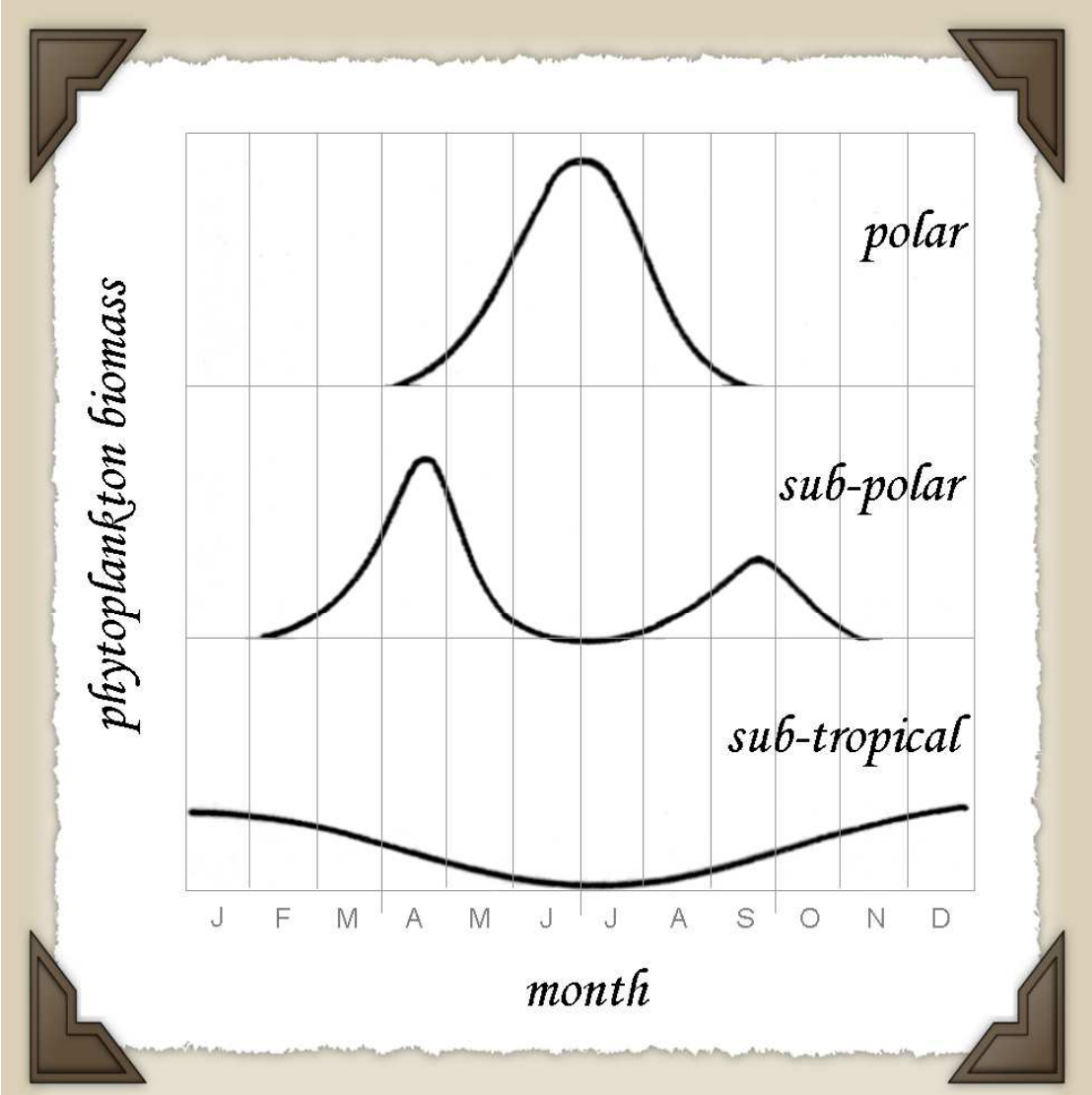

Cushing, D.H. (1959) "The seasonal variation in oceanic production as a problem in population dynamics". Journal du Conseil, CIEM Conseil International pour l'Exploration de la Mer / ICES International Council for the Exploration of the Sea, vol. 24, no. 3, p. 455–464.

Plate 2. Annual cycles of phytoplankton biomass, at different latitudes, as described by a simple conceptual model introduced by Cushing (1959). The months order, from January (J) to December (D), follows the seasonal sequence of the northern hemisphere. The modern latitudinal designation of a basin as "sub-tropical/sub-polar/polar" substitutes the original "tropical/temperate/arctic".

Plate 3. Seasonality of the Ligurian-Provençal Sea

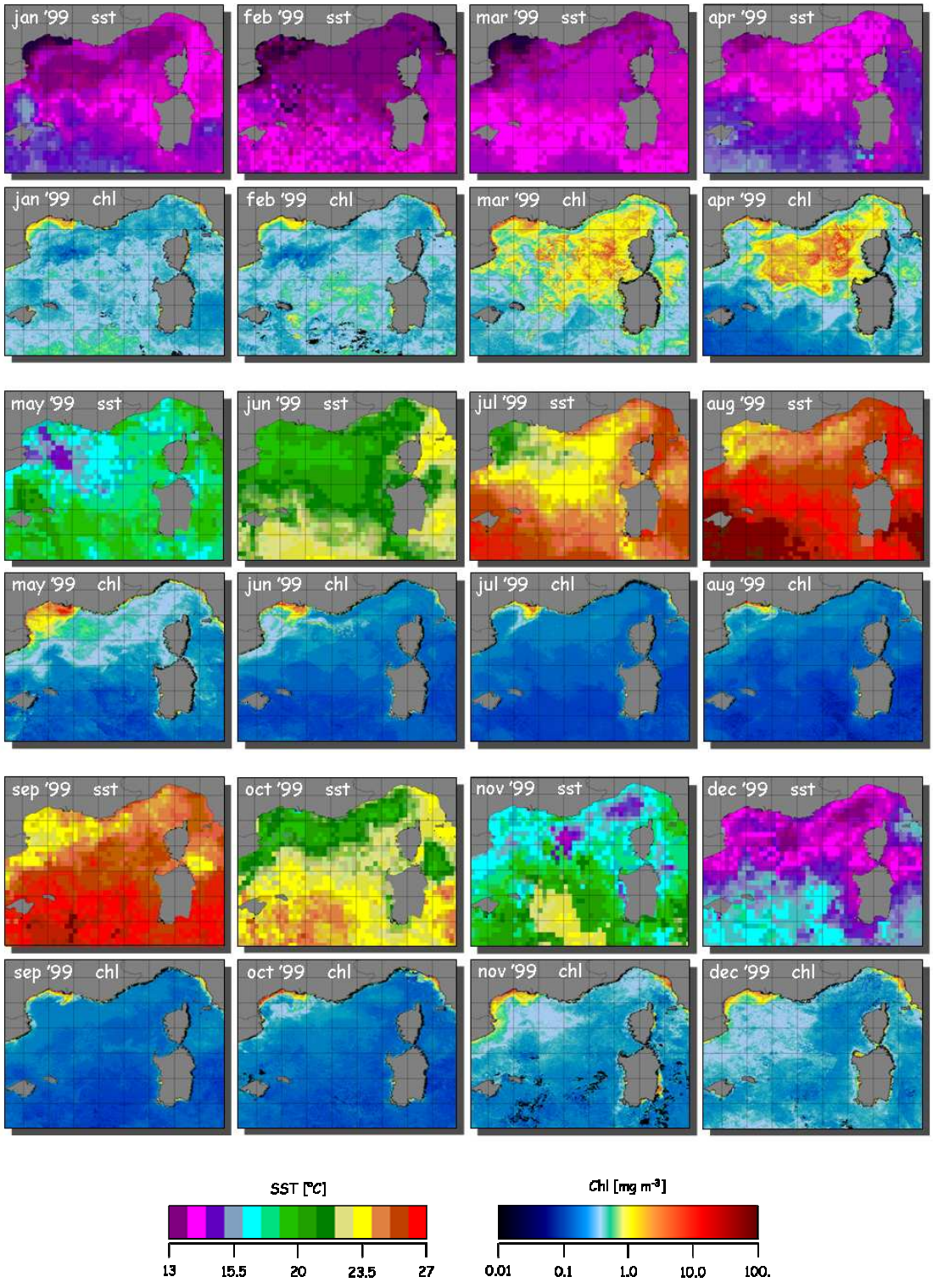

Plate 3. Sea surface temperature (SST) from ATSR1/2 and chlorophyll-like pigment concentration (Chl) from SeaWiFS, 1999 monthly means.

Plate 4. The Gulf of Lion environmental hotspot

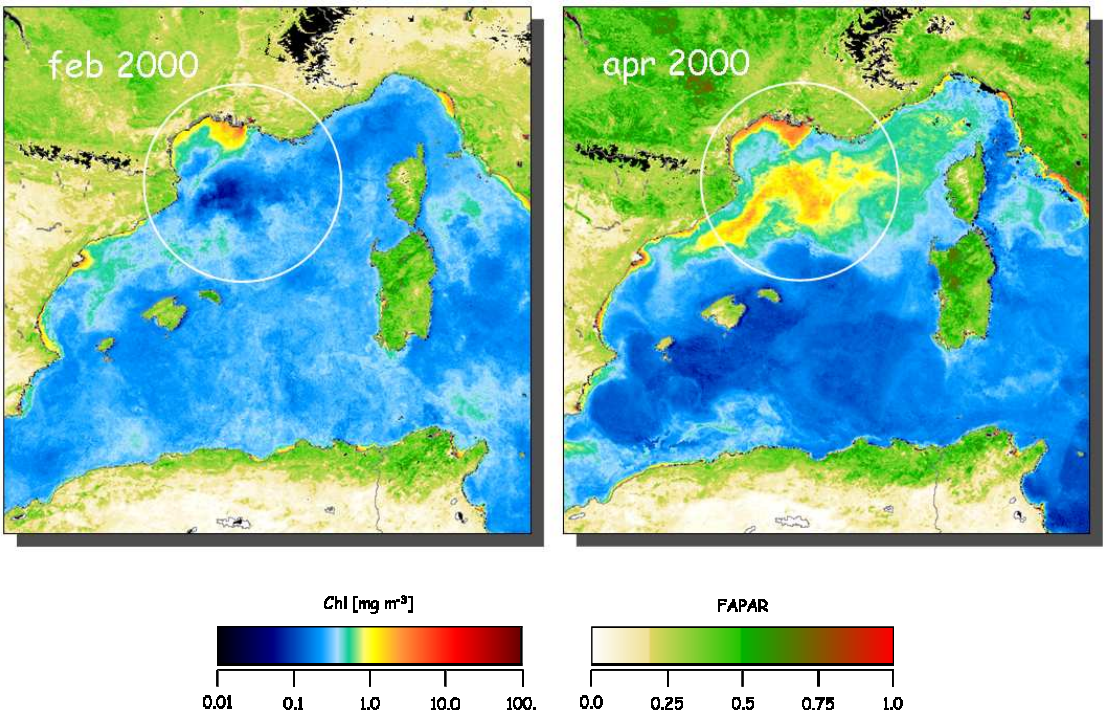

Plate 4. Ecological response to variable seasonal forcing in the Ligurian-Provençal Sea. The images cover an area of about 1000 km x 1000 km, with 2 km pixel resolution, and show monthly means of SeaWiFS-derived parameters, for February 2000 (left panel) and April 2000 (right panel). The colour coding represents: over water areas, a phytoplankton biomass indicator – *i.e.* chlorophyll-like pigment concentration, Chl [mg m^{-3}], derived from SeaWiFS data (JRC processing) – and, over land areas, a vegetation index – *i.e.* the Fraction of Absorbed Photosynthetically Active Radiation, FAPAR [dimentionless], also derived from SeaWiFS data (JRC processing). The surface features observable in the Gulf of Lion environmental hotspot (white circle, both panels) illustrate the "clearing" effect of deep convection in February, which generates the so-called "blue hole" appearing in the image, and the ensuing spring bloom, when the water column stabilizes, in April.

2. Data Sources

The combined use of diverse remote sensing and ecological modelling techniques, to assess complementary environmental data, provides novel opportunities for studying coastal and marine processes. Here, a comparison of SeaWiFS, CZCS, ATSR1/2, AVHRR and QuikScat data, collected in (at least partially) overlapping periods between 1997 and 2007, was used to study the coupling between algal blooms, other physical properties of the water surface (*e.g.* temperature) and wind patterns in the Ligurian-Provençal Sea. The model simulations performed with the GETM, coupled with GOTM, were used to generate times series of mixed layer depth and temperature corresponding to the available remote sensing data sets.

2.1 Chlorophyll-like Pigment Concentration (*Chl*) Data Sets

The SeaWiFS mission has generated an extensive collection of world-wide optical remote sensing data, since its start in September 1997. Ten consecutive full-year cycles, were considered here, to follow *Chl* dynamics in the Ligurian-Provençal Sea. The original imagery collected by the sensor was processed to correct top-of-the-atmosphere radiances of atmospheric noise, to derive normalized water-leaving radiances L_{WN}, and then to compute from these all other derived parameters, including *Chl*. Two data sets, derived from the same original SeaWiFS imagery, respectively by the National Aeronautics and Space Administration (NASA)[1], from September 1997 to August 2007, and by the Joint Research Centre (JRC)[2], from January 1998 to December 2007, have been used in the present study. In both cases, each processed image was re-mapped on a common equal-area grid, with a grid cell, or "bin", resolution of approximately 9 km for the NASA-provided Global Area Coverage (GAC) data and 2 km for the JRC-provided Local Area Coverage (LAC) data. Monthly and yearly composite data products were obtained from the re-mapped data, using all valid pixels for a given time period and grid cell to generate a weighted mean (based on the number of valid pixels used in the binning process). Further, climatological monthly/ yearly means were computed as the average of the corresponding monthly/yearly means derived for each of the 10 years in the series.

A single *Chl* average value, representative of the whole area of interest, was extracted from each monthly mean (and climatological) composite,

[1] Processed data are available from the **G**ES-DISC (Goddard Earth Sciences Data and Information Services Center) **I**nteractive **O**nline **V**isualization **AN**d a**N**alysis **I**nfrastructure (**Giovanni**) at http://disc.sci.gsfc.nasa.gov/giovanni/index.html. For details see http://oceancolor.gsfc.nasa.gov/REPROCESSING/SeaWiFS/R5.1/.

[2] Processed data are available from the **E**nvironmental **M**arine **I**nformation **S**ystem (**EMIS**) at http://emis.jrc.ec.europa.eu/. For processing and algorithms details see http://oceancolour.jrc.ec.europa.eu/.

as the mean of all pixels in the image subset bounded by 3.5-7.5°E and 40.5-42.5°N (see maps in Section 3, Plate 9). These average values can be used to compare the two SeaWiFS-derived data sets used – labeled "NASA data set" and "JRC data set" hereafter – for the subsequent analyses. The two time series, shown in Plate 5, provide substantially similar, albeit not identical, *Chl* values for the sites and times considered. Given that original data and processing algorithms are nearly the same in both cases, any divergence between the two data sets can only originate from differences in either the bad-data rejection scheme (*e.g.* the JRC data set does include image edges, where abnormal pixel size and inaccurate atmospheric correction might introduce some bias in the final product), or in the compositing process. The linear regression of monthly mean values in the overlap period, shown in Plate 6, indicates that the NASA data set tends to overestimates *Chl* in the high value range, with respect to the JRC data set. The correlation, however, remains very high (R^2 = 0.9035) and supports the adoption of either data set in different applications.

The use of composite data products also deserves some justification, given that SeaWiFS-derived daily images at full resolution (~1.2 km at nadir) display a larger amount of detail, and variability, in the patterns described by the *Chl* tracer. Contrary to composites, single images may be incomplete, over a given area, for long periods, because of imaging geometry, algorithm failure or cloud cover, even with daily overpasses of a wide-swath sensor like SeaWiFS. Hence the choice of using monthly/yearly means, to assess the main characteristics of surface waters from a statistical point of view (Antoine, 2004). Since the number of valid pixels increases with larger and longer binning intervals, the compositing process generates complete, cloud-free images. As will be seen, however, the variability due to highly dynamical events in a given area is averaged out too by the compositing process, which retains only those values and patterns that persist over significant areas and periods of time.

Finally, it should be recalled that the SeaWifs-derived indicators of ecological dynamics presented here must be considered with caution, owing to the presence of various coloured water constituents (and in part to bottom reflection, in shallow waters), which may significantly alter the signal derived from the sensor measurements, particularly in near-coastal areas (Gregg and Casey, 2004). The presence of optically active materials (*i.e.* dissolved organic matter and suspended inorganic particles) other than phytoplankton and related pigments, with partially overlapping spectral signatures, in particular, can prevent the computation of reliable *Chl* absolute values. However, when the limitations above are taken in due account, the analysis of historical time series of satellite data can provide accurate, if qualitative, information on recurrent algal blooms, and related environmental boundary conditions (Sathyendranath, 2000).

2.2 Sea Surface Temperature (*SST*) Sample Data

The 1999 *SST* sample data, shown in Plate 2, originate from the ATSR-1/2 data set. The original ATSR imagery was processed to apply sensor calibration, to correct for atmospheric contamination, and to derive *SST* values, as detailed in Zavody *et al.* (1995). The composite data products shown (Plate 3) were obtained from re-mapped original images, using all valid pixels for a given time period and grid cell to generate a weighted mean, as in the SeaWiFS case.

The AVHRR data set originates from the AVHRR Pathfinder Version 5.0 SST Project (Pathfinder V5), a re-analysis of the AVHRR data stream developed by the Rosenstiel School of Marine and Atmospheric Science (RSMAS), University of Miami, and the NOAA National Oceanographic Data Center (NODC), in partnership with the NASA Physical Oceanography Distributed Active Archive Center (PO.DAAC)[3]. The original image data, processed to apply sensor calibration, correct for atmospheric contamination, and derive *SST* values, have been exploited by the Joint Research Centre (JRC)[4] to cover the main European basins, using a geographical grid with cell resolution of approximately 2 km. Again, the composite data products were obtained from the re-mapped images, for ten consecutive full-year cycles (from January 1998 to December 2007), using all valid pixels for each month and grid cell to generate a weighted mean. Finally, a single *SST* average value, representative of the usual area of interest (3.5-7.5°E, 40.5-42.5°N), was extracted from each monthly composite.

2.3 Wind Speed (*WS*) and Direction Data

The *WS* data were collected by the microwave scatterometer QuikScat, the third in a series of NASA scatterometers that operate at 14 GHz (Ku-band). Scatterometers transmit microwave pulses down to the Earth's surface and then measure the power that is scattered back to the instrument, and that is related to surface roughness. For water surfaces, the surface roughness is highly correlated with the near-surface wind speed and direction (Schroeder et al., 1982; Donelan and Pierson, 1987). Hence, wind speed and direction at a height of 10 meters over the ocean surface are retrieved from measurements of the scatterometer's backscattered power[5].

---

[3] For details about the NOAA/NASA AVHRR Oceans Pathfinder Program, including data access and exploratory and analysis software, see the "Pathfinder Version 5.0 User Guide" at http://www.nodc.noaa.gov/sog/pathfinder4km/userguide.html.

[4] Processed data are available from the **E**nvironmental **M**arine **I**nformation **S**ystem (**EMIS**) at: http://emis.jrc.ec.europa.eu/. For references on data processing and on algorithms details see http://emis.jrc.ec.europa.eu/5_3_references.php.

[5] QuikScat data are produced by Remote Sensing Systems and are sponsored by the NASA Ocean Vector Winds Science Team. Details and processed data available at http://www.remss.com/.

The QuikScat standard processing produces daily and time averaged (3-day, weekly, monthly) gridded data files, by mapping the scatterometer orbital data to a 0.25 deg longitude by 0.25 deg latitude Earth grid. The composite data products used here, for comparison with the SeaWiFS data (limited to the period from 2000 to 2007), are monthly means re-mapped to the 0.25 degree grid. In the imagery shown (see section 4, Plate 13), overlaid to the colour-coded maps of *WS* are black arrows denoting the mean surface wind direction on a 0.5 degree grid. The wind speed values represent scalar averages of the daily data, while the wind directions are vector averages of the same data source. A single *WS* average value, representative of the whole area of interest, was extracted from the series of monthly composites (from which a climatological value was also derived).

2.4 Model-derived Data

The GETM/GOTM[6] configuration for the Mediterranean Sea used in this study corresponds to the version 1.7.x of the model, which has an horizontal resolution of 2' x 2' and 25 vertical layers, within a time window from January 1985 to December 2007. The model domain is extended westward beyond the strict Mediterranean domain to longitude 9°W, in order to allow mimicking of the Atlantic water inflow that enters the model domain through the Strait of Gibraltar, as well as the Mediterranean water outflow at depth. Also, the current GETM set up prescribes the Bosphorus Strait to be closed. Given that this narrow passage has a minimal width of only 1.5 km, its influence can be simulated with an inflow that is prescribed to be fresher than seawater in the same area. In practical terms, the Bosphorus inflow is treated in a way similar to that used for a fluvial discharge in the basin. The current configuration of the model includes 18 rivers (plus the Bosphorus). The corresponding fluvial discharges are climatological data from the Global River Data Center (GRDC) database[7] (see *e.g.* Looser *et al.*, 2007). In the current setting of the model, the fluvial discharges climatological cycle repeat every year with no inter-annual variations.

The GETM runs for the Mediterranean Sea are forced at the surface with European Center for Medium-Range Weather Forecast (ECMWF) data[8], the horizontal resolution of which is downscaled to 0.5°. The model is forced every 6-hours, *i.e.* at the frequency offered by the ECMWF datasets. Up to August 2002, atmospheric forcing data from

[6] The actual GETM code, as well as setup examples, can be found at http://getm.eu, while details on GOTM can be found at http://gotm.net.

[7] More details on available GRDC data products and new database developments can be found at http://www.bafg.de/GRDC/Home/homepage__node.html.

[8] More details on the available ECMWF data can be found at http://www.ecmwf.int.

the ECWMF re-analysis (ERA40) are used, while after that date the normal analyses from the operational forecasts are applied. Fluxes of momentum, heat and moisture are calculated internally from the meteorological variables provided. A feedback mechanism is implemented by using the SST of the last model time step for calculating the new fluxes.

The bathymetric grid is build using ETOPO1[9], a 1 arc-minute global relief model of the Earth's surface that integrates land topography and ocean bathymetry (Amante and Eakins, 2008), by averaging and smoothing to the corresponding horizontal resolution. The salinity and temperature climatologies, required at the start of the model integration, are taken from the MEDAR/MEDATLAS database (Maillard *et al.*, 2005), originating from the MEDAR/MEDATLAS II Project[10]. The resolution of the available climatological fields is 0.2°. No tidal forcing is included in the model results presented here.

[9] ETOPO1 grids are available at http://www.ngdc.noaa.gov/mgg/global/global.html.

[10] Deatails about the MEDAR/MEDATLAS II Project, as provided by IFREMER, can be found at http://www.ifremer.fr/medar/, while the integrated database developed is available on CD-ROM from http://www.ifremer.fr/medar/cdrom_database.htm.

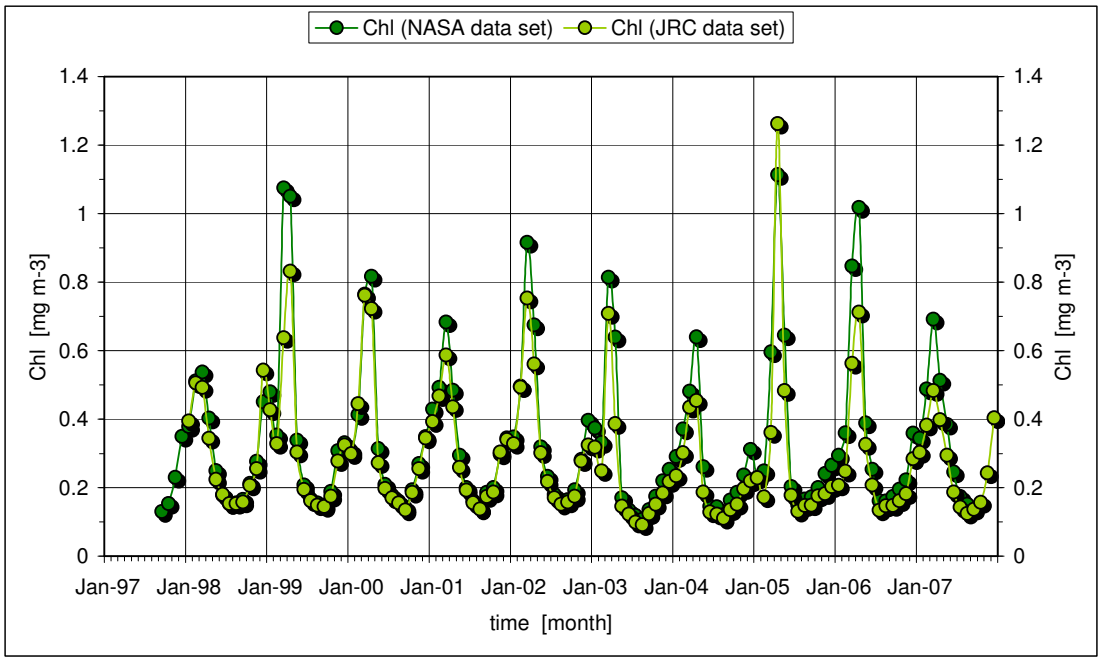

Plate 5. Time series of the *Chl* average values extracted from the monthly composites of the two SeaWiFS-derived data sets used (labeled "NASA data set" and "JRC data set"), as the mean of all pixels in the image subset bounded by 3.5-7.5°E and 40.5-42.5°N.

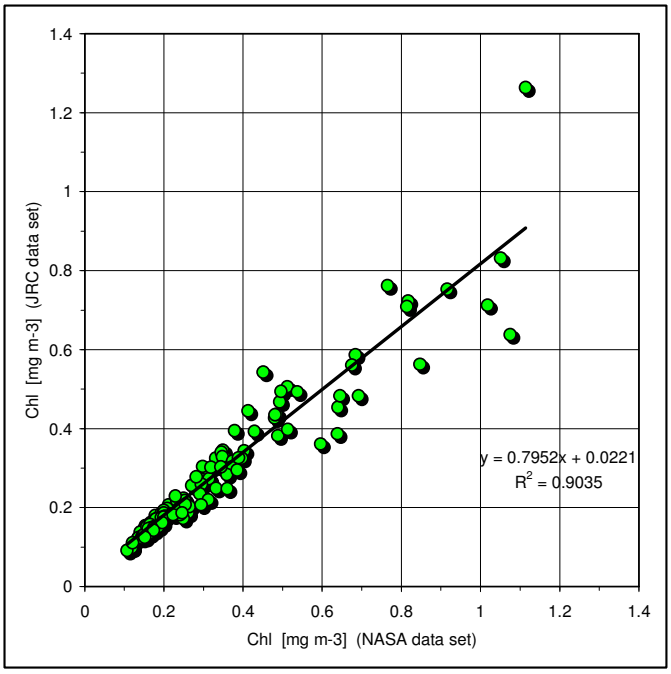

Plate 6. Linear regression of the *Chl* average values [mg m^{-3}] extracted from the monthly composites of the two SeaWiFS-derived data sets used (labeled "JRC processing" and "NASA processing"), as the mean of all pixels in the image subset bounded by 3.5-7.5°E, 40.5-42.5°N.

3. The SeaWiFS Chl historical time series

The *Chl* climatological yearly mean, for the entire Mediterranean Sea, computed over 10 annual cycles (September 1997 to August 2007) from the SeaWiFS (NASA) data set, is shown in Plate 7. The Ligurian-Provençal Sea emerges from the climatological map as a distinct region, where *Chl* mean values in the pelagic zone are among the highest of the entire basin (while, in general, coastal zones around the basin present values a factor 2 higher).

The *Chl* climatological monthly means, for the Ligurian-Provençal Sea, computed over the full annual cycle (September to August), from the same SeaWiFS (NASA) data set, are shown in Plate 8. The series illustrates the development of a (late fall and) winter bloom – with lower *Chl* values appearing in January and February across the Gulf of Lion area associated with the deep convection site – followed by a major spring bloom in March and April. The bloom is seen to decay afterwards and disappears in (late spring and) summer.

Plate 9 shows the image subset (3.5-7.5°E, 40.5-42.5°N) used for the extraction of a single *Chl* average value, representative of the whole area of interest, for each of the monthly means derived from the SeaWiFS (NASA) data set. The underlying maps in Plate 9 are the same climatological monthly means appearing in Plate 8, and demonstrate how the deep convection and blooming areas were both covered by the selected subset, while coastal and pelagic zones not involved in such processes were excluded from the analysis.

3.1 Time Series of *Chl* Monthly Averages

The full succession of *Chl* average values, computed over the image subset above, for each monthly mean in the 1997-2007 time series (NASA data set), is plotted – from September to August, for the 10 annual cycles considered – in Plate 10. The envelope of the annual curves shows again the *Chl* time sequence described earlier: fall and winter minor bloom, possible winter drop corresponding to the deep convection period, major spring bloom followed by the summer low.

The 2004-2005 curve presents the lowest winter values, in January and February 2005, and the strongest, but latest, blooming event in April 2005 (Plate 11, top panel). The very low *Chl* values of January and February 2005 correspond to the largest, and longer lasting, "blue hole" of the entire data set (see subset images in Plate 15, Section 4). Since it is believed that such a feature corresponds to the site of deep convection, it should be associated to a strong wind regime. As will be detailed later, the wind record over the north-western Mediterranean Sea, in late 2004 and early 2005, shows several months of *WS* well above the climatological value computed for the 2000-2007 period, with the highest intensity in February 2005 (see subset images in

Plate 14, Section 4). Apparently, this intense and exceptional episode of atmospheric forcing prevented any blooming off the Gulf of Lion, in early 2005. Since it is reasonable to presume that there is a significant time lag between atmospheric forcing and its effects on the ecosystem (as will be seen in Section 4), the prolongued period of vertical mixing delayed the 2005 spring bloom some, but it also increased nutrient availability to the point that, once the water column stabilized, the blooming reached unprecedented levels.

Such a "delayed-mode" blooming, with a peak in April, is not uncommon, in the 1997-2007 SeaWiFS data record, as it occurred also (albeit on a reduced scale) in 1999, 2000, 2004 and 2006 (Plate 11, middle panel). Note that an "early-mode" blooming, with a peak in March, occurred just as often, during the period considered here, in 2001, 2002, 2003 and 2007 (plate 11, bottom panel). The only serious anomaly, with respect to this bi-modal pattern, occurred in 1998, when NO "blue hole" formed in winter (see images in Plate 15, Section 4), and the peak of the early spring bloom, in March, was about the lowest of the entire data set (Plate 11, top panel). It would be interesting to see whether the wind record (not available in the QuikScat time series used here, which starts in the year 2000) could confirm that a reduced atmospheric forcing failed to trigger the deep convection, and hence the nutrient enrichment that should have fostered a spring bloom, during that winter. Further, it may be appropriate to mention that 1997-1998 was one of the strongest *El Nino* years on record, which brought record high winter temperature to many areas in Europe (Rodwell *et al.*, 1999). Such anomalous temperatures might have contributed to reduce deep convection in the 1997-1998 winter and limit the 1998 spring blooming.

Plate 12 shows the climatological *Chl* area-averaged values, derived from the monthly means in the 1997-2007 time series (NASA data set) plotted in Plate 10, over the same September-to-August annual cycle. Anticipating the comparison with the wind speed record, to be discussed in Section 4, the climatological *WS* area-averaged values, derived from the monthly means in the 2000-2007 QuikScat data set, has been added to the same plot for comparison. The climatological curves show that the increasing *Chl* values in fall correspond to increasing wind speed, but that *Chl* does not grow further in winter when *WS* reaches its maximum values (responsible for the deep convection and associated nutrient enrichment processes). Then, the major spring bloom accompanies a substantial drop in wind speed, and is followed by the summer low of both *Chl* and *WS*.

As will be detailed in Section 4, the comparison of the area-averaged *Chl* and *WS* time series of monthly means, indicates that there's only a weak correlation (at least at the time scale considered) between the two parameters, when they correspond to the same time interval. Indeed, it will be seen that the correlation is almost non-existent, if

one considers concurrent values, *i.e.* a 0 months time lag between the two measurements, while it grows with increasing time lag, it reaches a maximum, in a few months, and then drops again. This suggests that the wind regime of late fall, early winter is critical for the pre-conditioning of the deep convection area, the entire Ligurian-Provençal Sea in fact, and in determining when the blooming will occur, and how intense it will be, in the following spring.

3.2 Long-term trend: the historical CZCS record

Interestingly enough, the historical CZCS climatological monthly means (Plate 13) show that, in the period 1979-1985, the feature we referred to as the "blue hole" started to appear already in December, and then recurred systematically in January, February AND March. The spring bloom appeared only in April, and continued in May. Again, it would be interesting to assess the differences, if any, in the wind field of the late 1970's, early 1980's over this region, with respect to that of the late 1990's, early 2000's. Is global warming currently increasing the surface temperature of the Mediterranean Sea, and therefore anticipating the onset of stratified condition (as well as the spring bloom in the north-western basin)? Recent analyses of AVHRR-derived *SST* in the last 30 years seem to support this idea (Nykjaer, 2008). If this was the case, then, a stronger stratification would also imply a lower rate of nutrient enrichment in the surface layer, and a reduced *Chl* concentration (across the basin). More questions arise from this hypothesis: were the winters preceding the "early-mode" blooming (with peak in March) in 2001, 2002, 2003 and 2007 particularly warm, so as to justify an anticipated onset of the stratification? And, ultimately, is the available *Chl* time series long enough, and accurate enough, to see a significant trend in the basin-wide mean *Chl*, consequent to the climate warming effect?

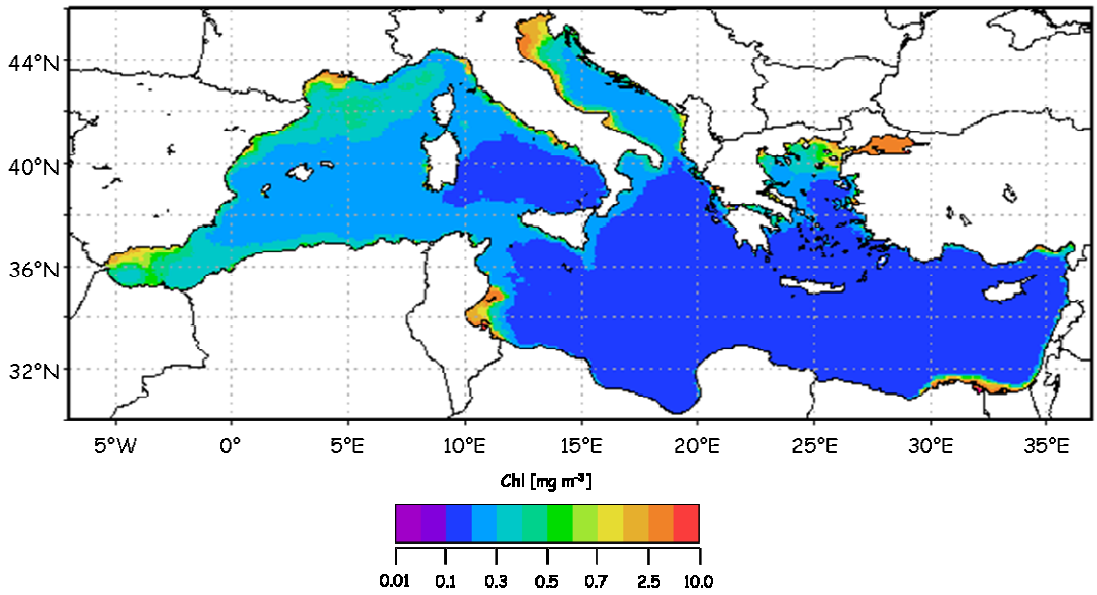

Plate 7. Mediterranean Sea. Climatological yearly mean, over 10 seasonal cycles (September 1997 to August 2007), of chlorophyll-like pigment concentration, *Chl* [mg m^{-3}], a phytoplankton biomass indicator derived from SeaWiFS data (NASA data set).

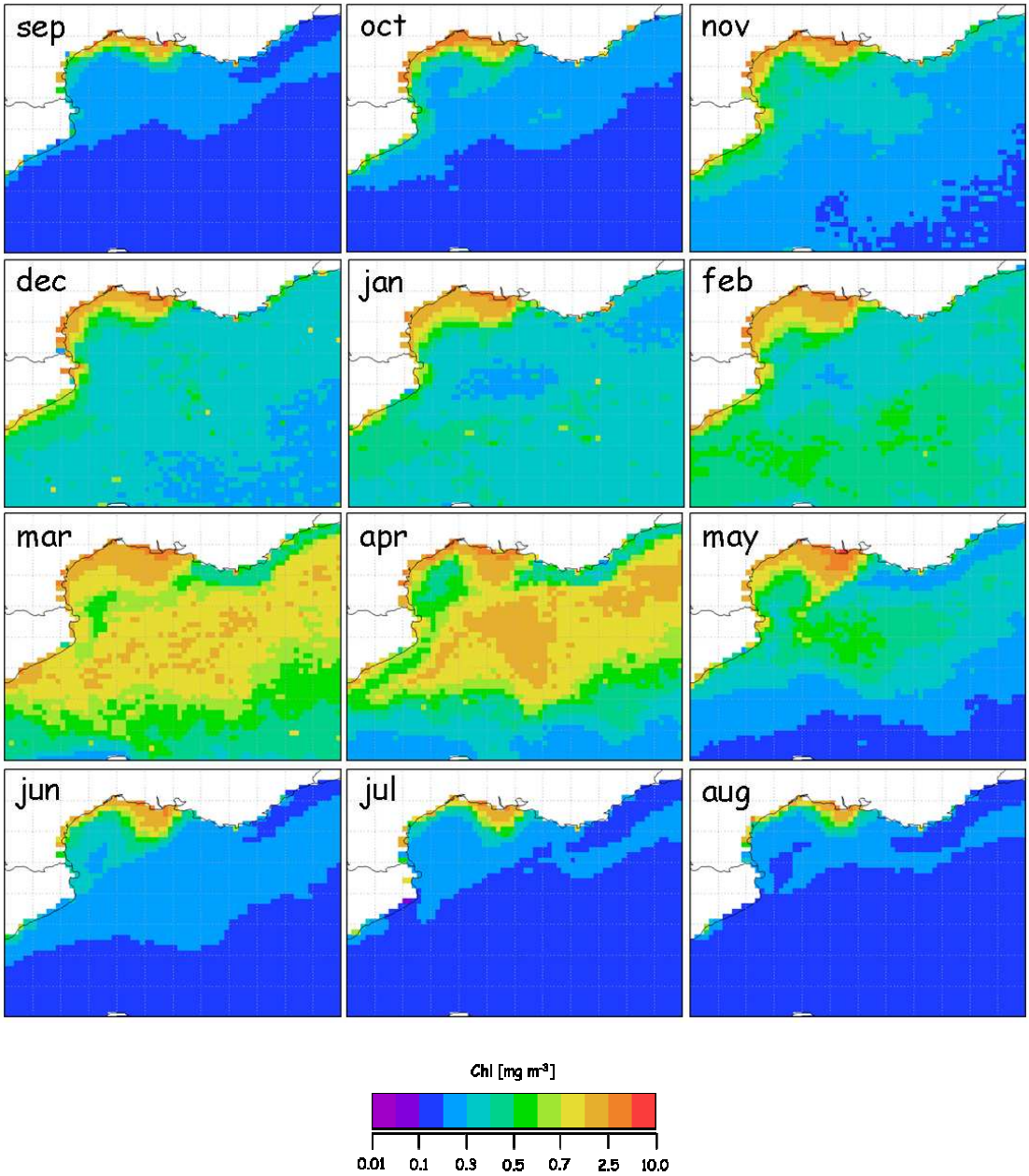

Plate 8. Ligurian-Provençal Sea. Climatological monthly means, over 10 seasonal cycles (September 1997 to August 2007), of chlorophyll-like pigment concentration, *Chl* [mg m^{-3}], a phytoplankton biomass indicator derived from SeaWiFS data (NASA data set).

Plate 9. Gulf of Lion, area of interest for statistical analysis

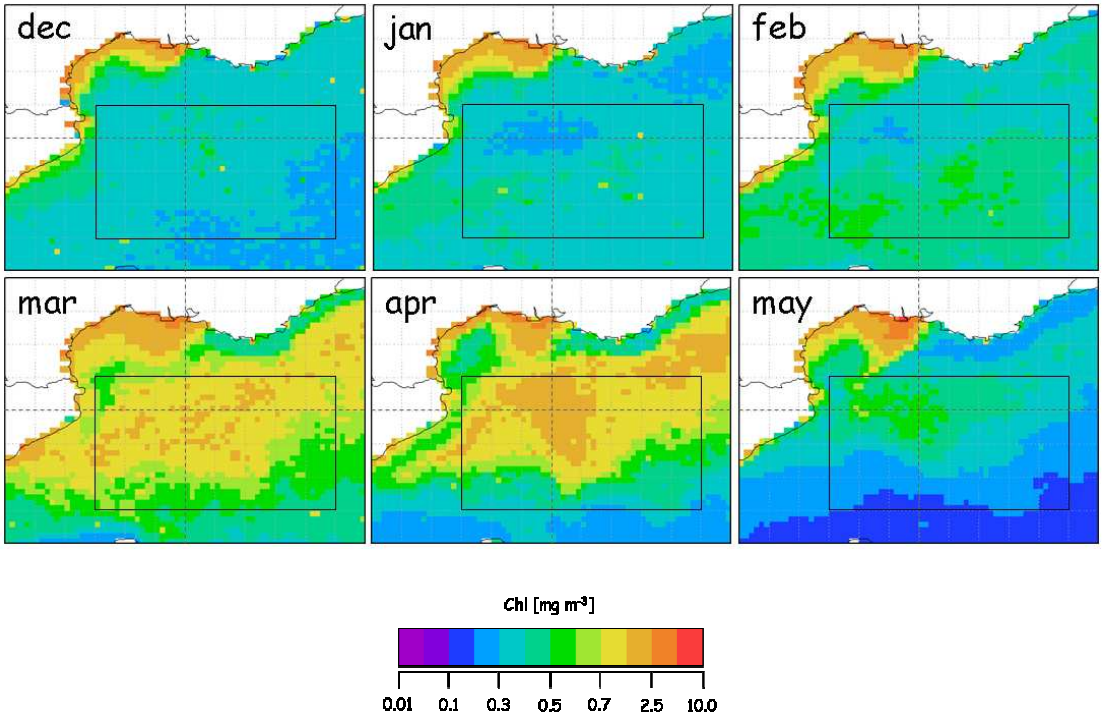

Plate 9. Ligurian-Provençal Sea. The black box represents the area of interest (3.5-7.5°E, 40.5-42.5°N) used for the subsequent analysis of area-averaged *Chl* values. The dotted lines cross at 5°E, 42°N, considered to be the conventional center of the site where winter deep convection takes place. The underlying maps are the climatological monthly means, over 10 seasonal cycles (September 1997 to August 2007), of chlorophyll-like pigment concentration, *Chl* [mg m^{-3}], a phytoplankton biomass indicator derived from SeaWiFS data (NASA data set).

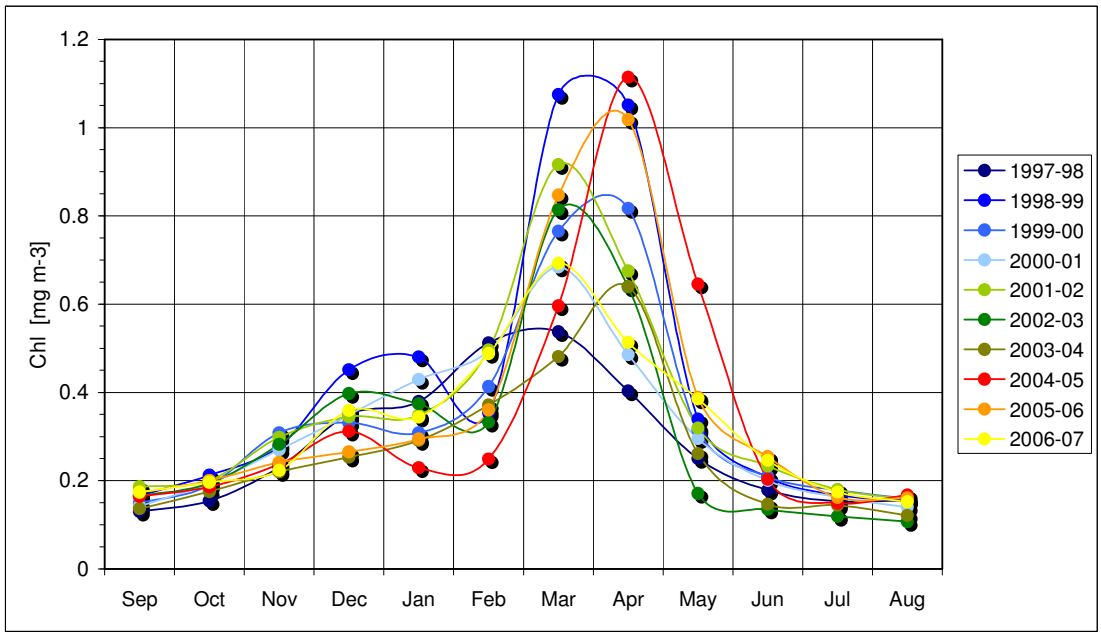

Plate 10. Inter-annual variability of *Chl* area-averaged values, computed over the image subset 3.5-7.5°E, 40.5-42.5°N, for each of the monthly means in the SeaWiFS-derived (NASA data set) 1997-2007 time series.

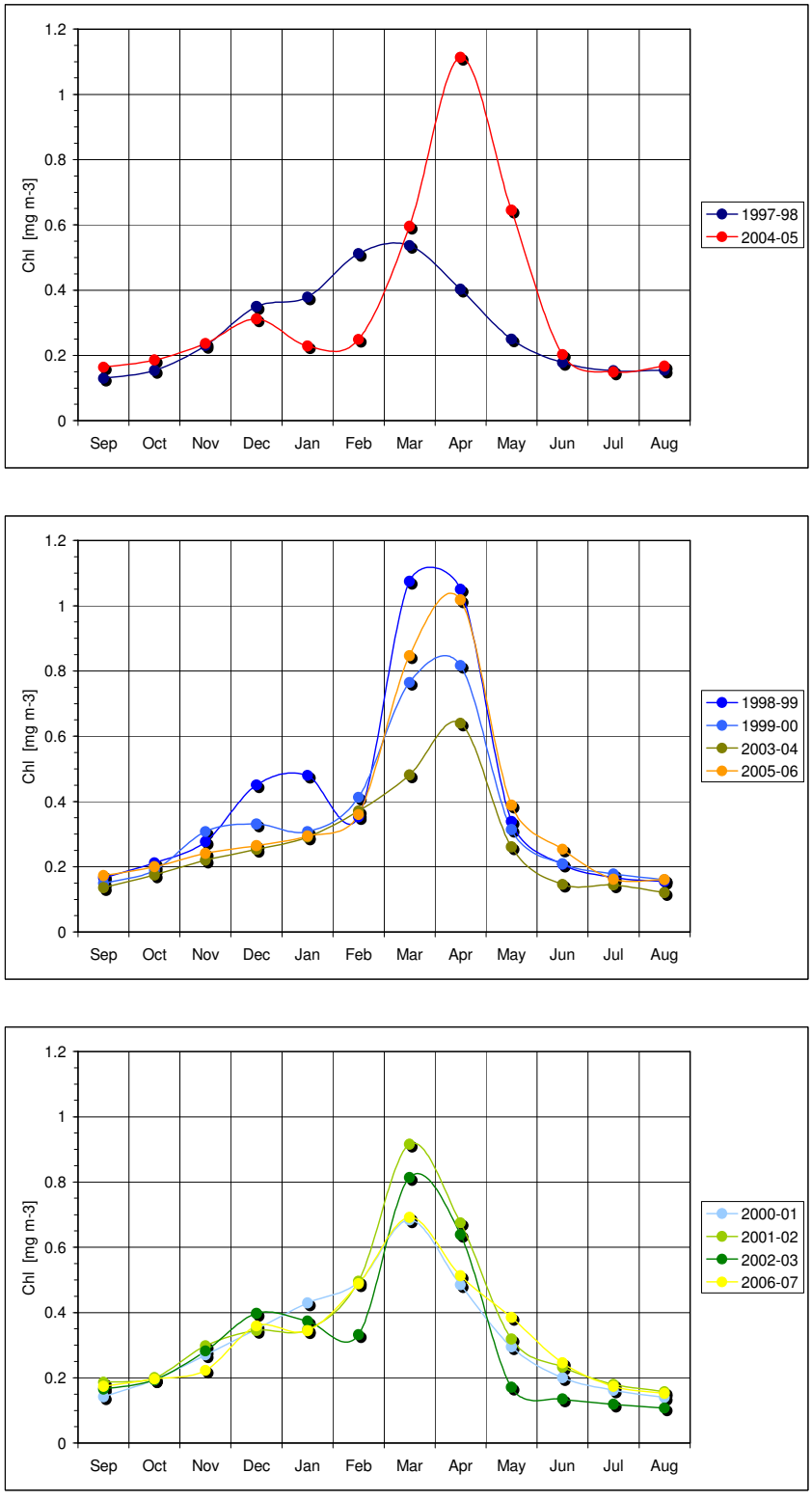

Plate 11. Inter-annual trends of *Chl* area-averaged values, computed over the image subset 3.5-7.5°E, 40.5-42.5°N, for each of the monthly means in the SeaWiFS-derived (NASA data set) 1997-2007 time series.

Plate 12. Chl and WS area-averaged climatological values

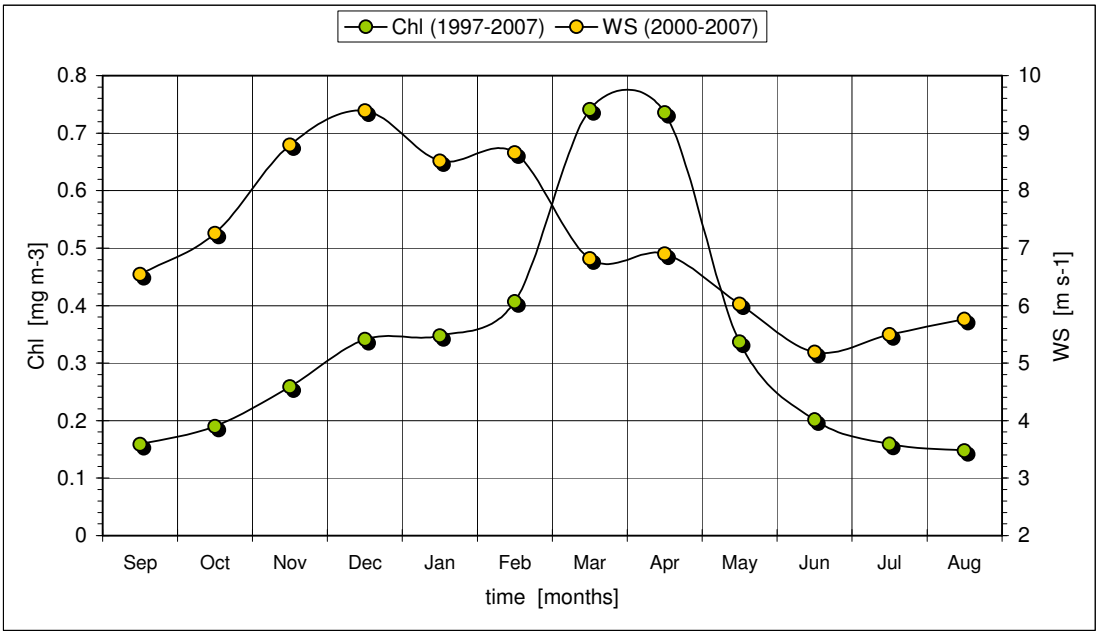

Plate 12. Monthly climatologies of *Chl* and *WS* area-averaged values, computed over the subset 3.5-7.5°E, 40.5-42.5°N, and derived respectively from the 1997-2007 SeaWiFS (NASA) data set and the 2000-2007 QuikScat data set.

Plate 13. Mediterranean Sea, CZCS Chl annual climatology

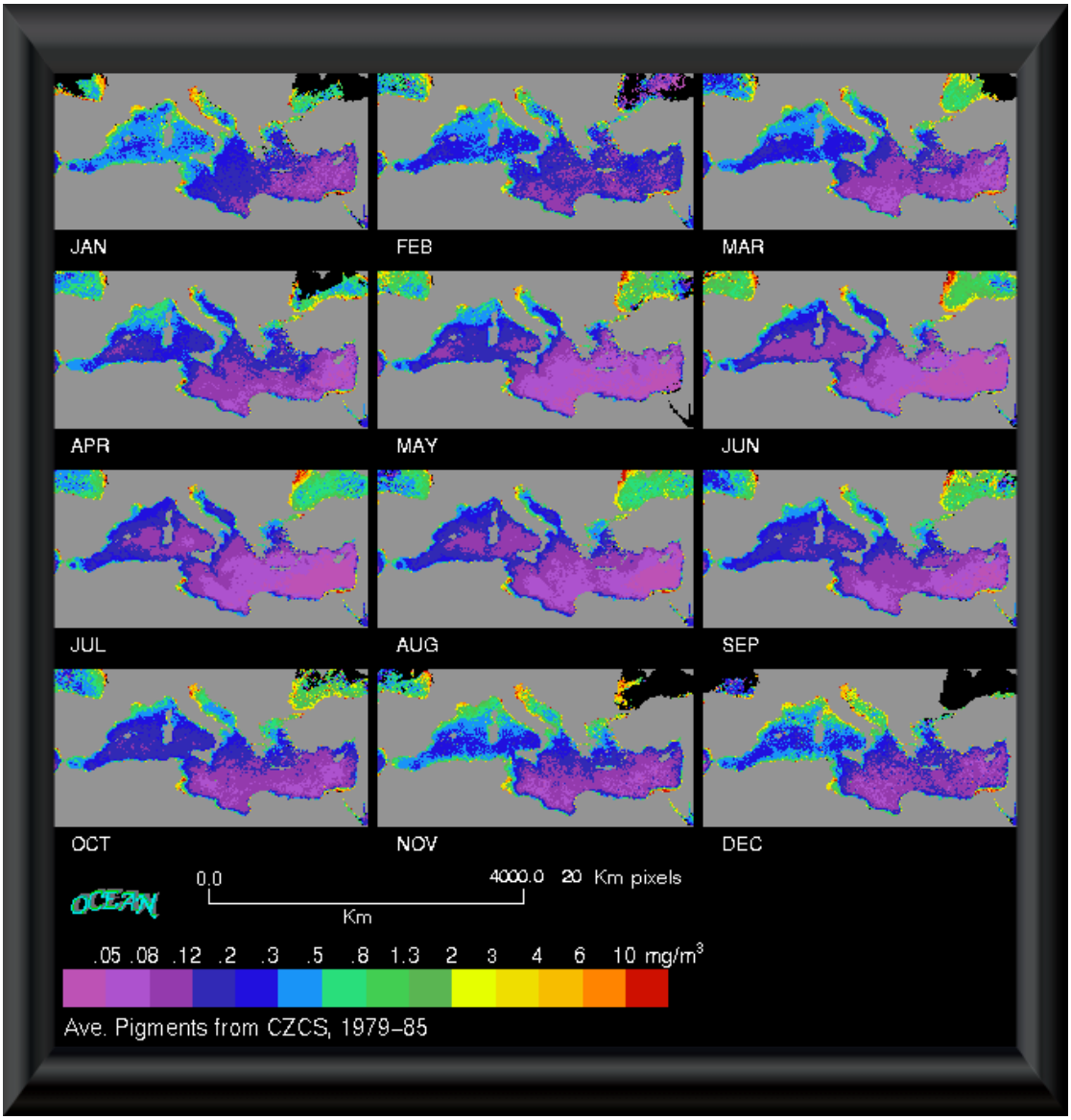

Plate 13. Mediterranean Sea. Climatological monthly means, over 7 seasonal cycles (January 1979 to December 1985), of chlorophyll-like pigment concentration, *Chl* [mg m^{-3}], a phytoplankton biomass indicator derived from CZCS data (JRC processing).

4. Comparison of algal blooms and wind patterns

The surface wind fields over the Ligurian-Provençal Sea, computed from the Quikscat data set, are shown in Plate 14, while the corresponding surface pigment fields, determined from the SeaWiFS (NASA) data set, are shown in Plate 15. Both Plates comprise only the sub-series of monthly means – of *WS* (and direction) and *Chl* – from January through May, for the years from 2000 to 2007. The monitoring period of these sub-series, limited to the years in which both kinds of data were available, was chosen to capture the development of the classical "blue hole" and spring bloom sequence in the Gulf of Lion area. As discussed earlier, the features recurring in this near-coastal hotspot represent the main blooming events of the entire Mediterranean Sea, not driven directly by continental runoff (as the Rhone plume presents separate dynamics; see the *Chl*-traced river plume spreading south-westward in Plate 13).

The full succession of *Chl* and *WS* area-average values, computed over the usual image subset, for each monthly mean in the 2000-2007 time series, is plotted in Plate 16 (upper panel). The *WS* record shows that maxima are reached systematically in the fall-winter period, *i.e.* between November and February. The highest winds occur in November/December ($WS \sim 10$ m s^{-1}), at times in January/February, with absolute peaks in November 2001, January 2003 and February 2005 ($11 < WS < 12$ m s^{-1}). The fall-winter maximum are followed by lower values ($6 < WS < 8$ m s^{-1}) in spring, from March onwards, and then by the lowest values ($WS \sim 5$ m s^{-1}) in summer. Notable exceptions are January 2002 and January/February 2007, when the monthly means were below 6 and 8 m s^{-1} respectively, in the entire area, and then again April 2001, when values higher than 9 m s^{-1} were measured over the entire Gulf of Lion.

When these wind fields are compared with the corresponding pigment fields, higher *WS*, in January and February, correspond to lower pigment concentrations ($0.3 < Chl < 0.4$ mg m^{-3}), and often to the formation of a distinct "blue hole" ($Chl \sim 0.2$ mg m^{-3}), in the Gulf of Lion – although, at the monthly scale considered, the correspondence is not always evident and unambiguous, as suggested by the cases of early 2005 (high winds, large "blue hole") and early 2006 (low winds, even larger "blue hole"). Lower *WS*, from March onwards, correspond to strong blooming ($Chl > 1.0$ mg m^{-3}), as the *Chl* record always peaks in March-April. Finally, the lowest wind speeds, in summer, correspond to the lowest pigment concentrations (Chl ~ 0.2 mg m^{-3}).

The climatological area-averaged values of *WS* and *Chl*, computed for the chosen subset using the monthly means in the 2000-2007 time series, is also shown in Plate 16 (lower panel).

A simple regression analysis, carried out using the 2000-2007 average values plotted in Plate 16 (upper panel), is shown in Plates 17 and 18. Various time lags, from 0 to 6 months, were considered, in order to take into consideration the effect of two environmental factors: first, the biological response of the ecosystem cannot be instantaneous, after the set up of conditions favourable to algal growth (*i.e.* the increase in nutrient concentration due to vertical mixing); second, when the wind is strongest, the continuing deep convection can prevent blooming and lead instead to the formation of a "blue hole" in the pigment field. With no time lag (*i.e.* when each *Chl* average value is matched with the *WS* average value of the same month; see Plate 17, panel a), the linear fit shows essentially no correlation ($R^2 \sim 0$), while the second order polynomial fit ($R^2 = 0.05$) suggest that *Chl* is low at lower *WS*; it grows together with *WS*, but only up to a point; and then it drops again, as *WS* becomes higher and higher – a drop interpreted as corresponding to the occurrence of deep convection. As the time lag increases, so does the correlation (see the R^2 plot against time lag, for the first 6 cases considered, in Plate 17, panel b).

The lack of a significant correlation, when *WS* and *Chl* are matched with no time lag, is due essentially to the fact that the ecosystem of the Ligurian-Provençal Sea responds in a very distinct manner to the extreme atmospheric forcing typical of winter months. In fact, if the regression analysis of monthly mean values is restricted to the first 4 months of the year, the correlation is more significant ($R^2 \sim 0.28$, both in the linear and in the polynomial case), but negative, as shown in Plate 17, panel c. In other words, above a certain *WS* threshold, the higher the wind, the stronger the convection processes, the lower the pigment values in the surface layer. As already mentioned before, when *WS* increases above a certain value, and triggers the deep convection, the algae are mixed down to great depth in the water column, and cannot regain the surface to start over their photosynthetic activity. In this period, then, high *Chl* values occur only at lower *WS*. Conversely, for the remainder of the year, *i.e.* from May to December, the correlation is much, much lower ($R^2 \sim 0.07$, both in the linear and in the polynomial case), but positive, as shown in Plate 17, panel d.

The maximum correlation between *WS* and *Chl* is reached after 4 months (*i.e.* when each *Chl* average value is matched with the WS average value of 4 months before), with $R^2 \sim 0.3$ for both the linear and the polynomial fit (see Plate 18, panels a to d). At higher time lags, the correlation decreases again to very low values, *i.e* $R^2 \sim 0.01$, 0.02 (as already shown in Plate 17, panel b).

Plate 14. Monthly mean WS (Jan-May) in the Gulf of Lion

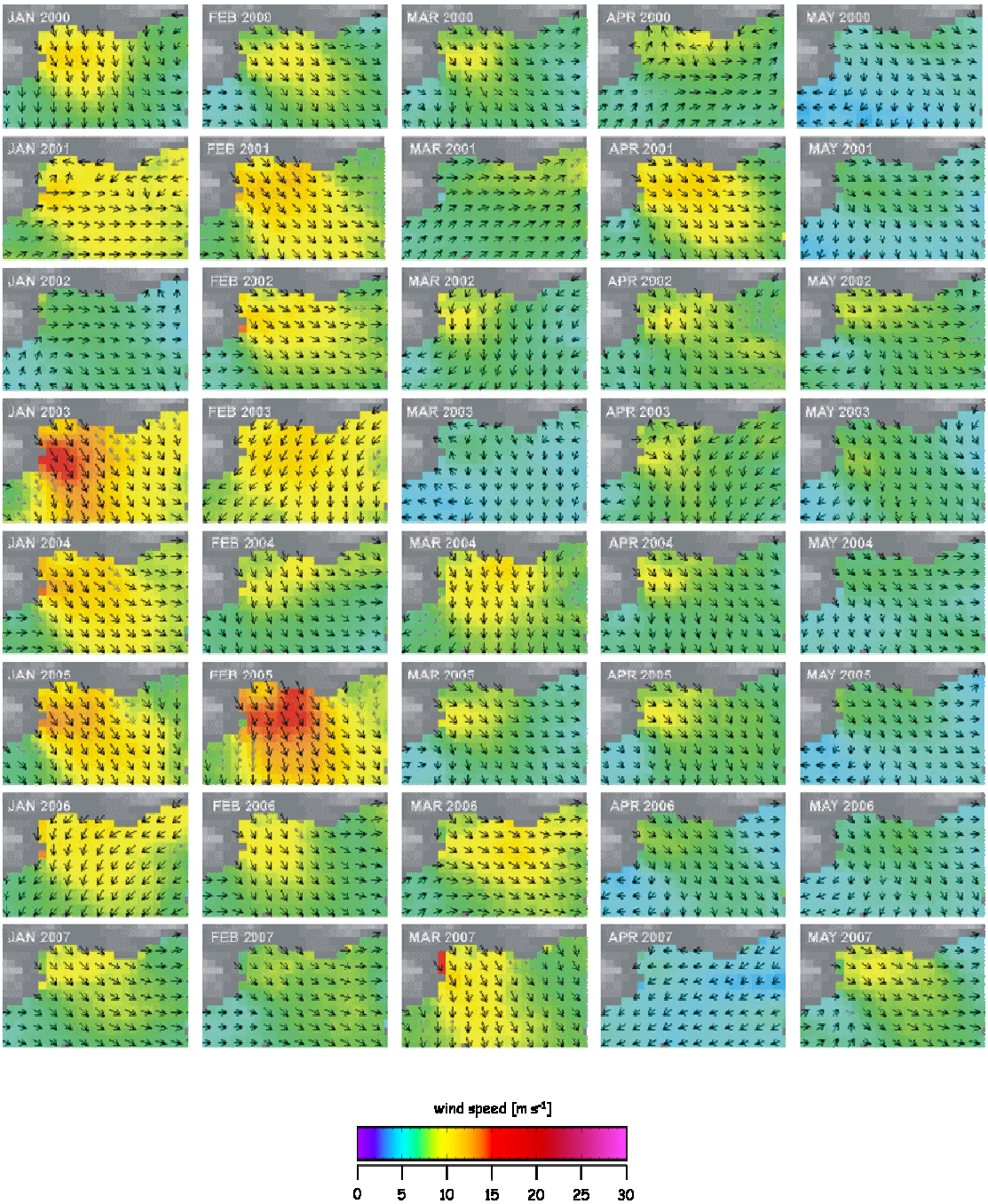

Plate 14. Ligurian-Provençal Sea. QuikScat-derived monthly mean *WS* [m s^{-1}], January through May (columns), from 2000 to 2007 (rows). The wind speed data were mapped on a 0.25 degree grid; the overlaid vectors denote the wind direction on a 0.5 degree grid.

Plate 15. Monthly mean Chl (Jan-May) in the Gulf of Lion

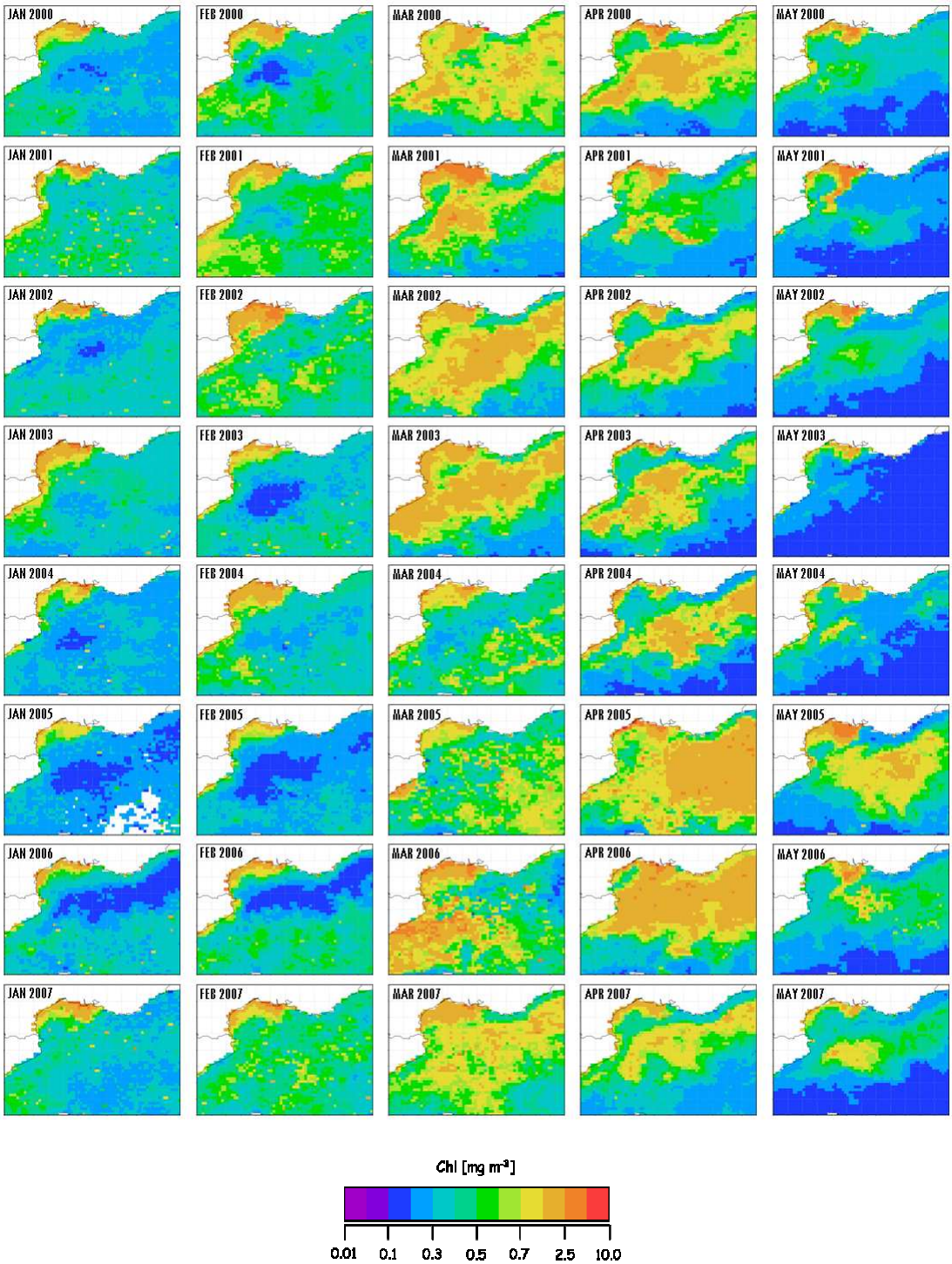

Plate 15. Ligurian-Provençal Sea. SeaWiFS-derived (NASA data set) monthly mean *Chl* [mg/m^3], January through May (columns), from 2000 to 2007 (rows).

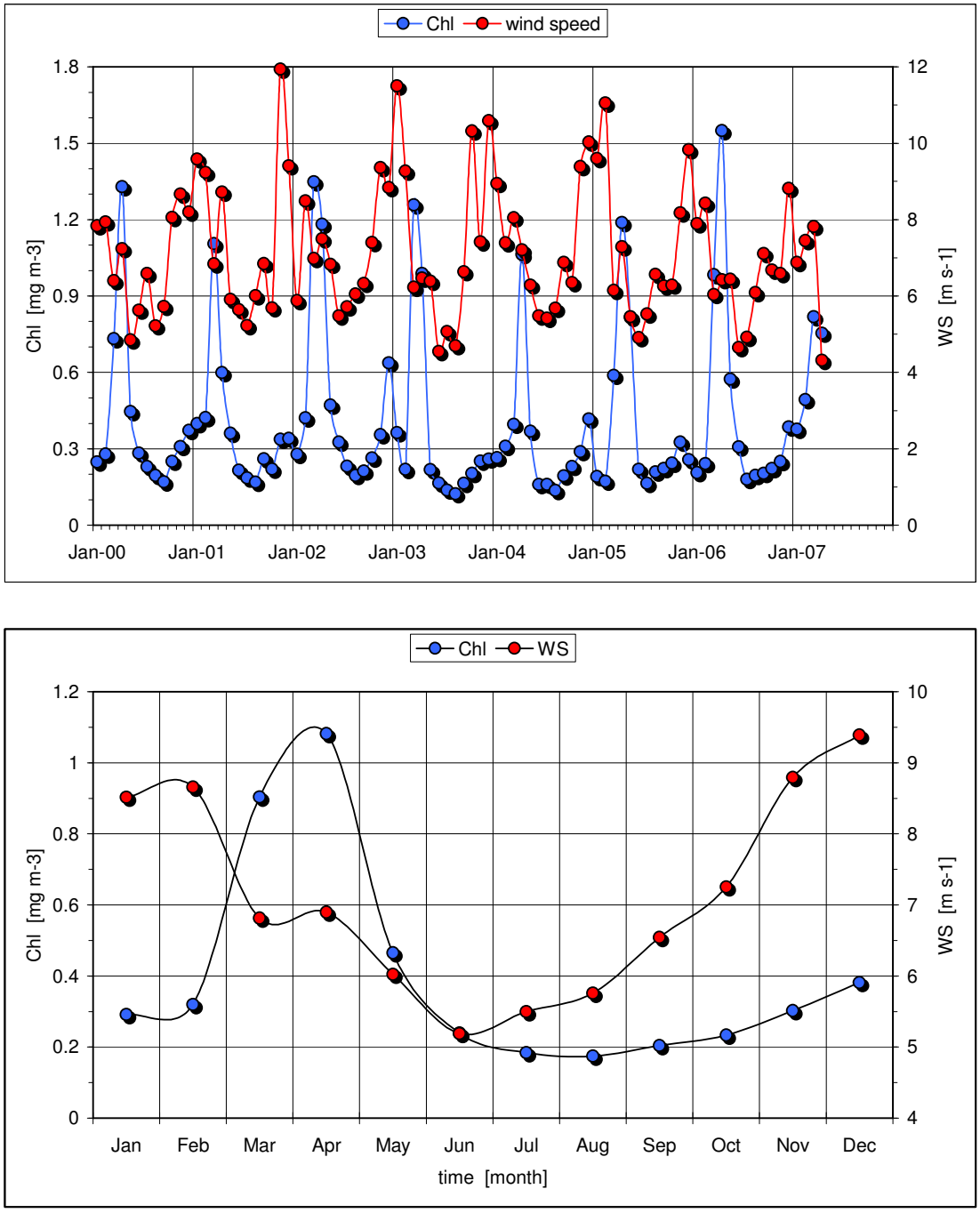

Plate 16. Time series for 2000-2007 (upper panel) and climatological monthly average values (lower panel) of *Chl*, computed from SeaWiFS-derived (NASA data set) monthly means, and of *WS*, computed from QuikScat-derived monthly means, for the Gulf of Lion.

Plate 17. Chl and WS 2000-2007 regression analysis (1)

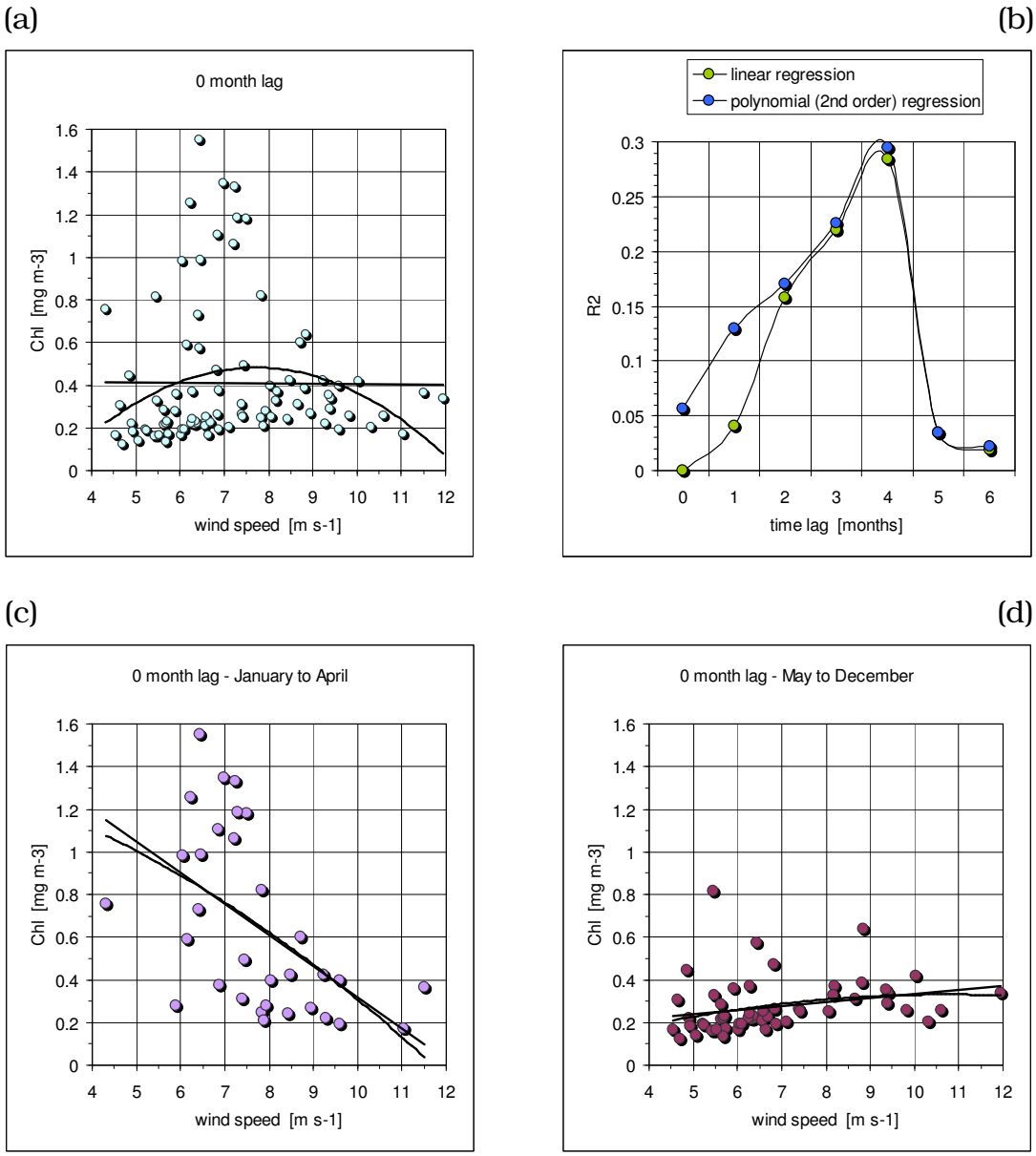

Plate 17. Panel a: regression analysis of *Chl* and *WS* monthly average values (2000-2007) in the Gulf of Lion, at 0 months time lag. Panel b: plot of R^2 values derived from linear/polynomial (2^{nd} order) regressions of *Chl* and *WS*, at successive time lags. Panel c: regression analysis of *Chl* and *WS* monthly average values in the Gulf of Lion, at 0 months time lag, for the period from January to April; and panel d: for the period from May to December.

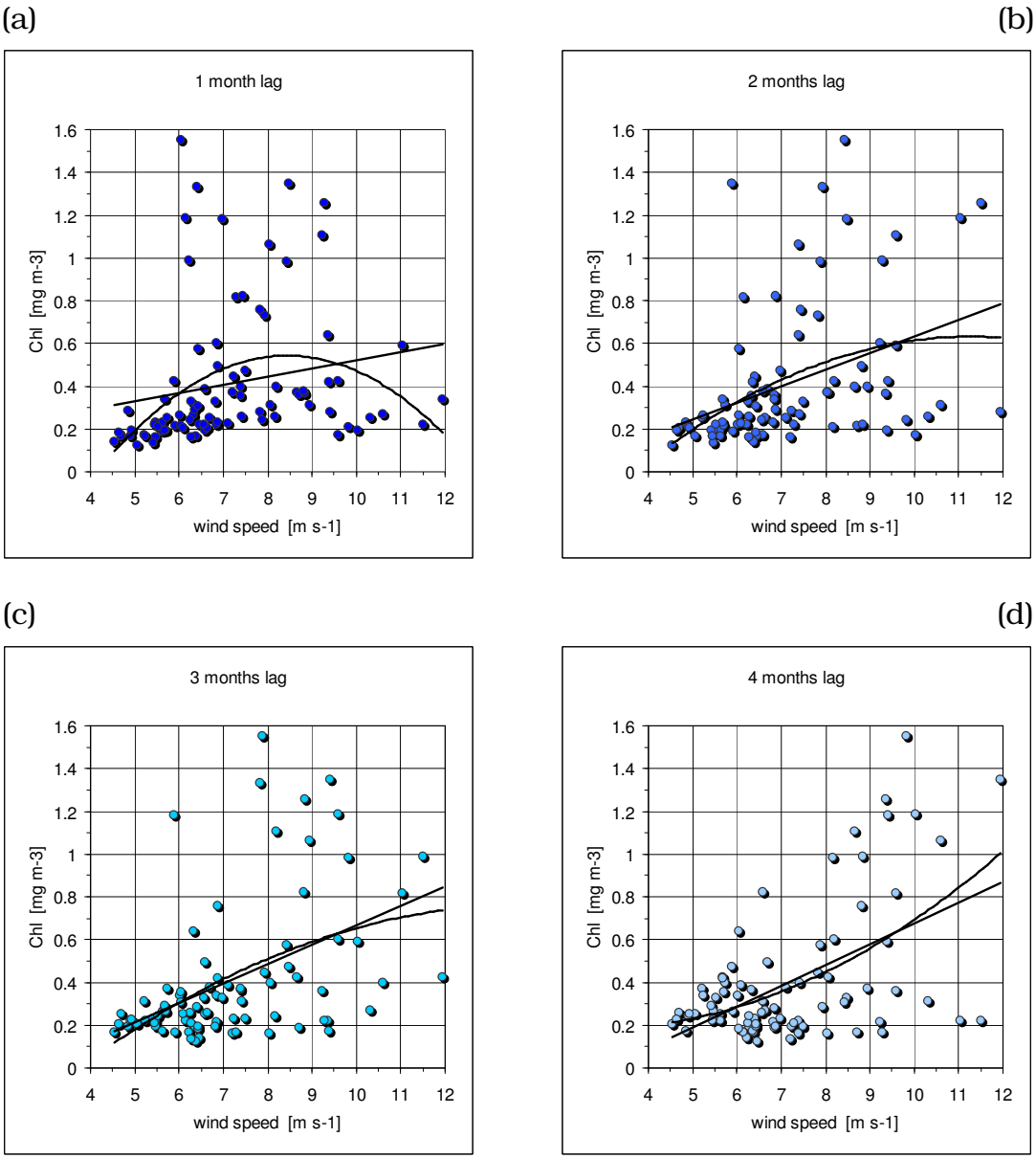

Plate 18. Regression analysis of *Chl* and *WS* monthly average values (2000-2007) in the Gulf of Lion, at successive time lags. Panel a: 1 month time lag. Panel b: 2 months time lag. Panel c: 3 months time lag. Panel d: 4 months time lag.

5. Comparison of satellite data and model results

The climatological monthly means of Mixed Layer Temperature (*MLT*) and Mixed Layer Depth (*MLD*) for the entire Ligurian-Provençal Sea, derived from the GETM output over the full annual cycle for the decade January 1998 to December 2007, are shown in Plate 19 and Plate 20, respectively. The two series – which can be compared directly with the September-to-August *Chl* series shown in Plate 8 – illustrate the onset of winter cooling, accompanied by a major deepening of the mixed layer in January, February and March.

The series of *MLT* and *MLD* monthly mean values, which characterize the water column in the Gulf of Lion, are plotted in Plate 21. The upper panel provides a comparison between AVHRR-derived *SST* and the corresponding GETM-derived *MLT*. In the middle and lower panels, the *SST* and *MLT* time series are compared with the corresponding GETM-derived *MLD*. As evident in the scatter plot of Plate 20 (upper panel), *SST* and *MLT* are highly correlated (R^2 = 0.965 for both linear fit and 2nd order polynomial fit). The main feature of the *MLD* and *SST* / *MLT* comparison, instead, is the low temperature that always accompany the deepening of the mixed layer, irrespectively of the depth reached. In the scatter plots of plate 22 (middle and lower panels), the *MLD* maintains a rather constant minimum value for a wide range of *SST* / *MLT*, and it is only when these approach 12 °C that the depth range increases substantially. The correlation indicated by a linear fit is very low, in this case (R^2 = 0.31 / 0.28, for *SST* / *MLT* respectively), but it improves with a 2nd order polynomial fit (R^2 = 0.47 / 0.43, for *SST* / *MLT* respectively).

These physical parameters can be compared with the SeaWiFS-derived (JRC data set) *Chl* values for the same period, as plotted in Plate 23. When *Chl* is matched up to either *SST* or *MLT*, the main feature emerging from the time series comparison is that blooming always follows a period of very low temperatures. The regression analysis of Plate 24 (upper and middle panels) shows that *Chl* (just like *MLD*) maintains a rather constant minimum value for a wide range of *SST* / *MLT*, and it is only when these approach 12 °C that the pigment concentration range increases substantially. The correlation indicated by a linear fit is very low, in this case (R^2 = 0.45, for both *SST* / *MLT*), but it improves again with a 2nd order polynomial fit (R^2 = 0.47 / 0.51, for *SST* / *MLT* respectively).

The comparison of the *Chl* and *MLD* time series, instead, appears to be more difficult to interpret. Once again, very high pigment concentrations always accompany the deepening of the mixed layer, but the trend is not always respected in the magnitude of the peaks. A shallow mixed layer may correspond to low *Chl* values (as in 1998 and 2007) or may not (as in 2002). A deeper mixed layer may correspond to higher *Chl* values (as in 1999, 2000, 2001 or 2003, 2005) or may

not (as in 2004, 2006). This lack of consistency in the general trend is reflected by the *Chl / MLD* scatter plot of Plate 22 (lower panel), where increasing *Chl* values seem to occur over a wide range of mixed layer depths, so that the correlation is very low (R^2 = 0.13 for the linear fit and R^2 = 0.30 for the 2nd order polynomial fit). As shown in Plate 23, the correlation increases at 1 month time lag (R^2 = 0.58 for the linear fit and R^2 = 0.58 for the 2nd order polynomial fit), but then drops at 2 months (R^2 = 0.32 for both linear fit and 2nd order polynomial fit) and disappears at 3 months (R^2 ~ 0 for the linear fit and R^2 = 0.07 for the 2nd order polynomial fit). As already seen in Section 4, this suggests that the biological response of the ecosystem is not instantaneous, after the set up of conditions favourable to algal growth, and that the development of a bloom seems to depend on the pre-conditioning fostered by a prolongued period of vertical mixing.

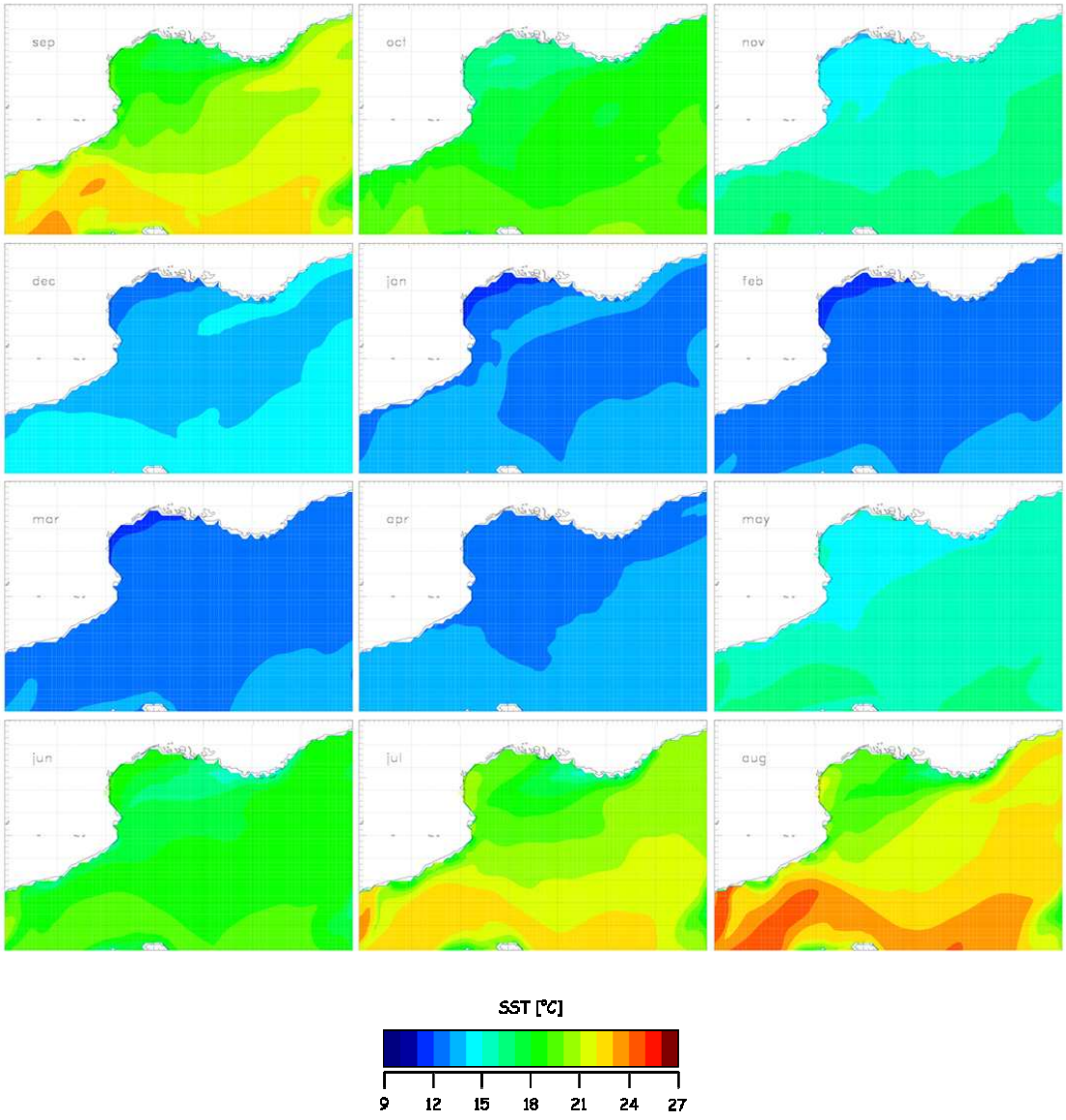

Plate 19. Ligurian-Provençal Sea. Climatological monthly means, over 10 seasonal cycles (1998 to 2008), of mixed layer temperature, *MLT* [°C], derived from the GETM.

Plate 20. Gulf of Lion, climatological mixed layer depth

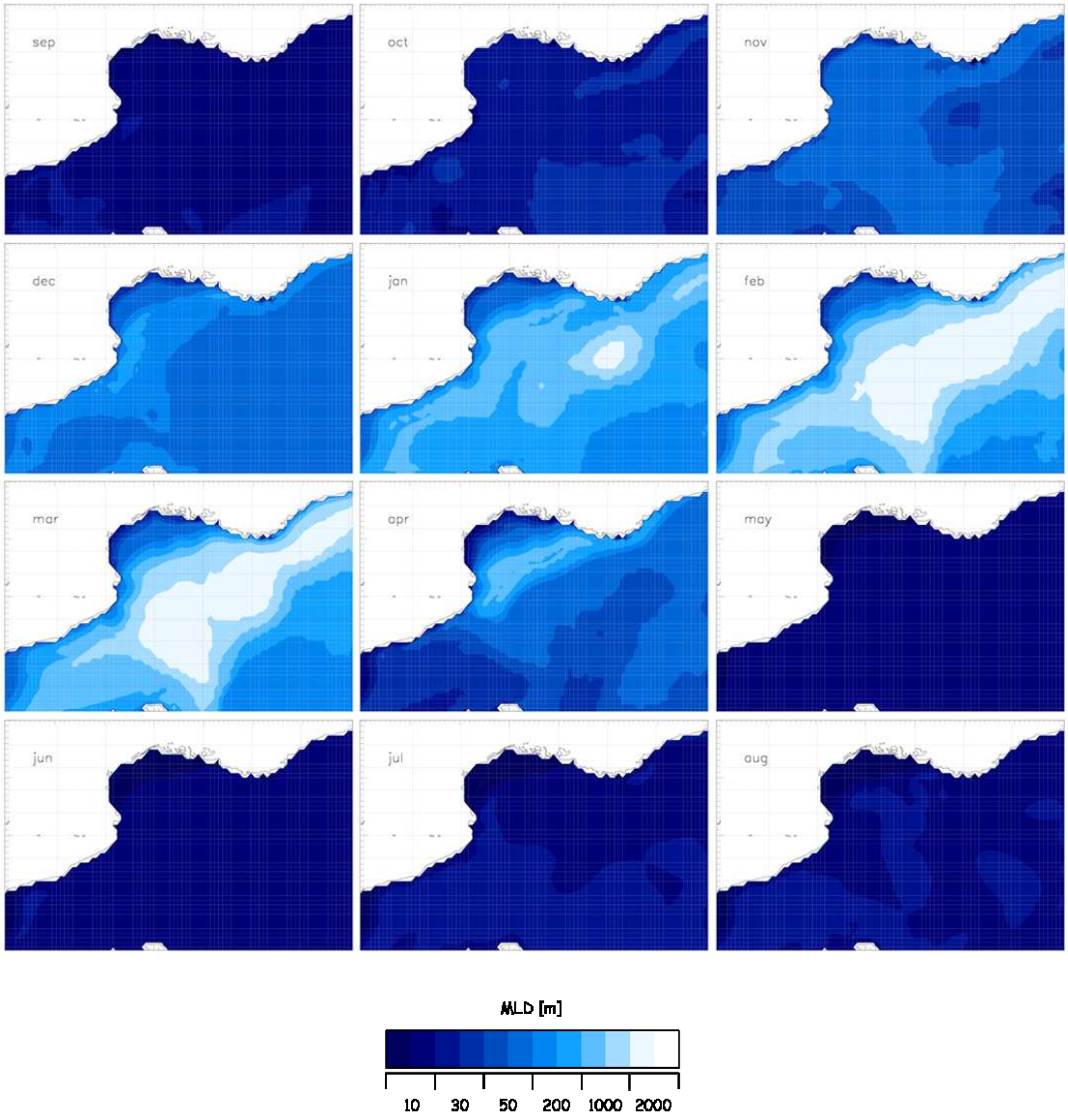

Plate 20. Ligurian-Provençal Sea. Climatological monthly means, over 10 seasonal cycles (1998 to 2008), of mixed layer depth, *MLD* [m], derived from the GETM.

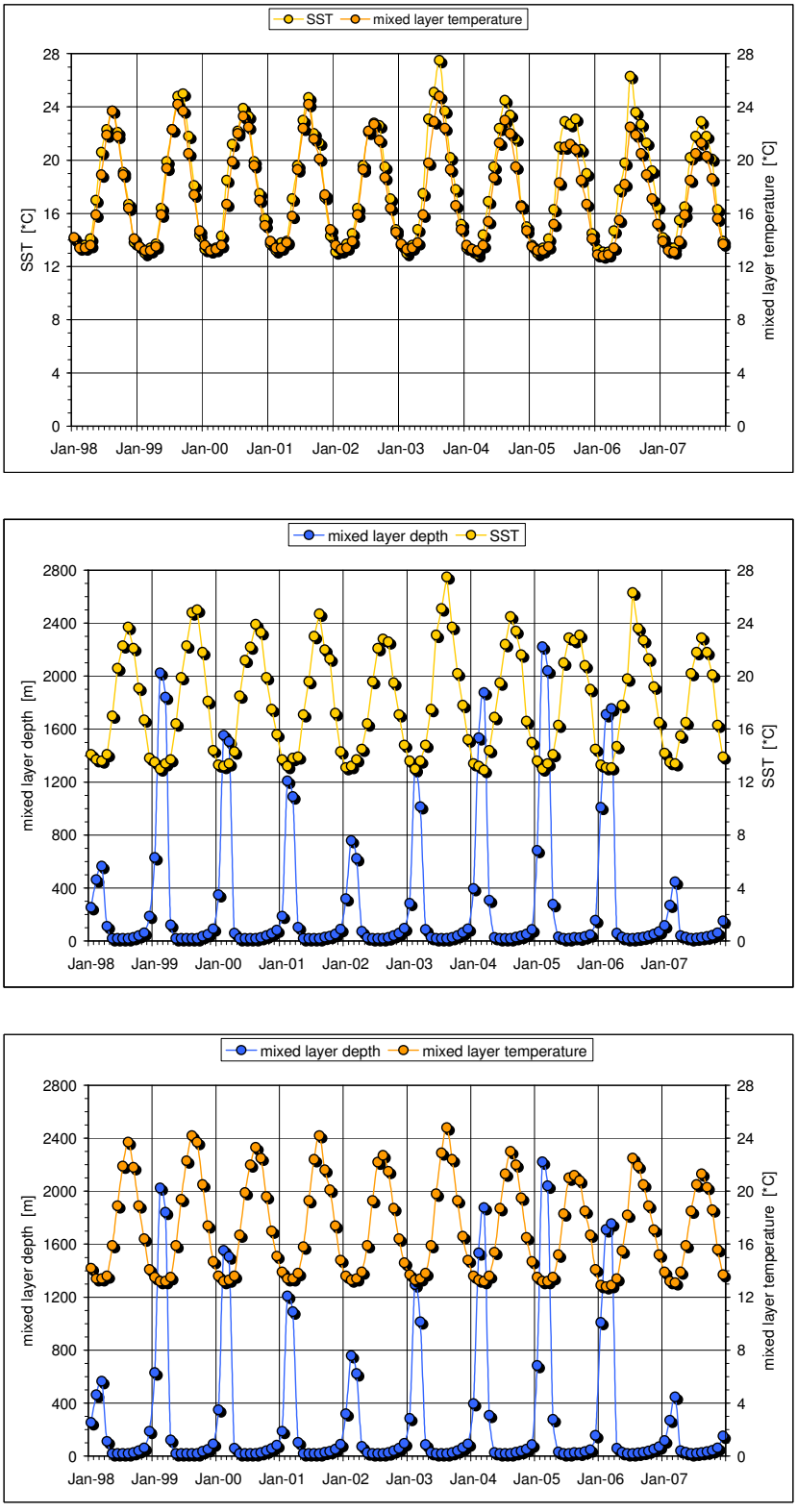

Plate 21. Time series (1998-2007) of AVHRR-derived *SST*, and GETM-derived mixed layer temperature (*MLT*) and depth (*MLD*); Gulf of Lion.

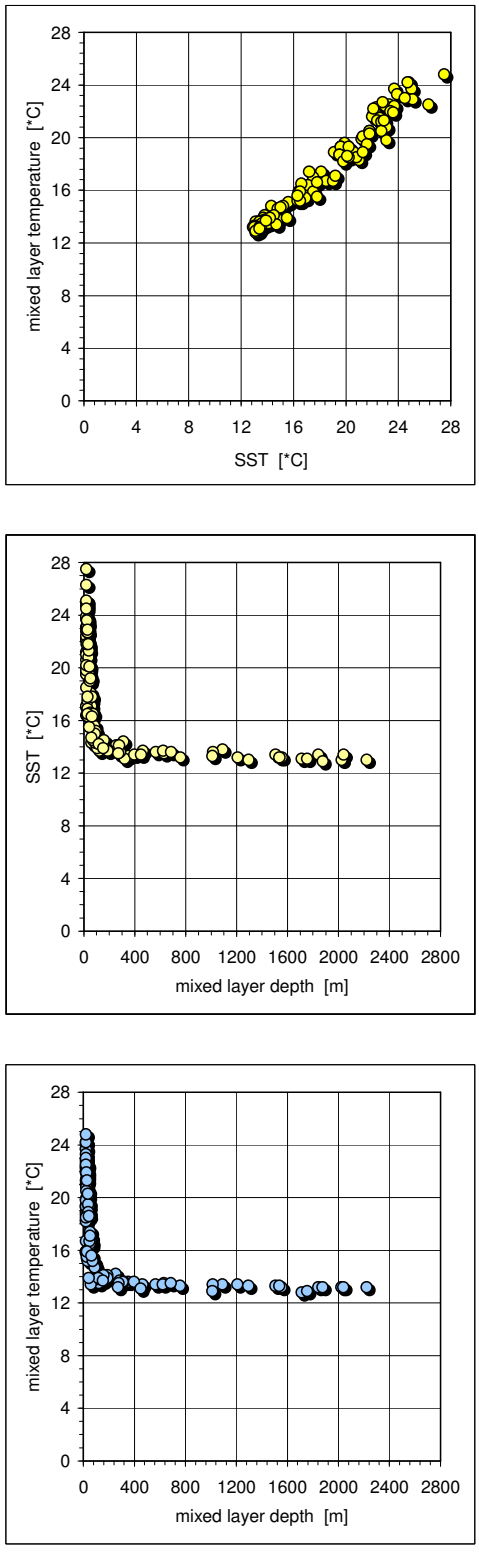

Plate 22. Scatter plots (1998-2007) of AVHRR-derived *SST*, and GETM-derived mixed layer temperature (*MLT*) and depth (*MLD*); Gulf of Lion.

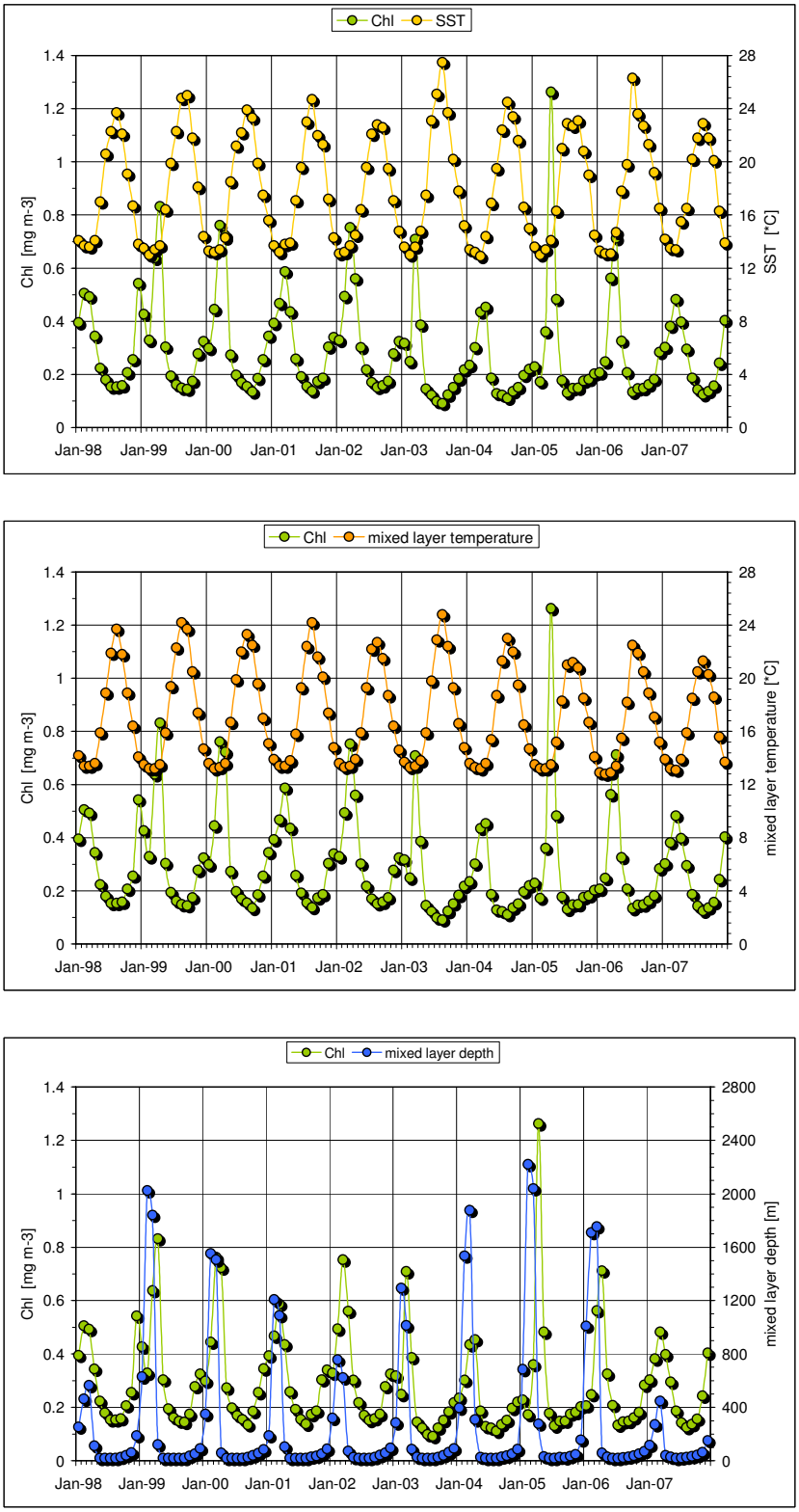

Plate 23. Time series (1998-2007) of SeaWiFS-derived (JRC data set) *Chl*, AVHRR-derived *SST*, GETM-derived *MLT* and *MLD*; Gulf of Lion.

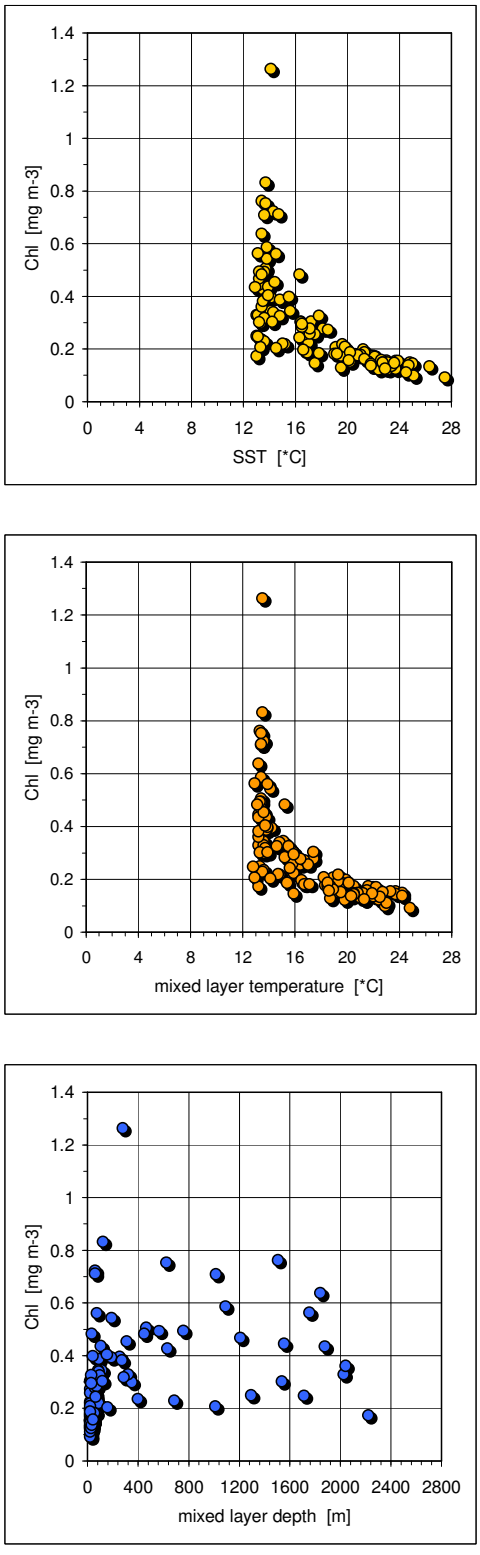

Plate 24. Scatter plots (1998-2007) of SeaWiFS-derived (JRC data set) *Chl*, AVHRR-derived *SST*, GETM-derived *MLT* and *MLD*; Gulf of Lion.

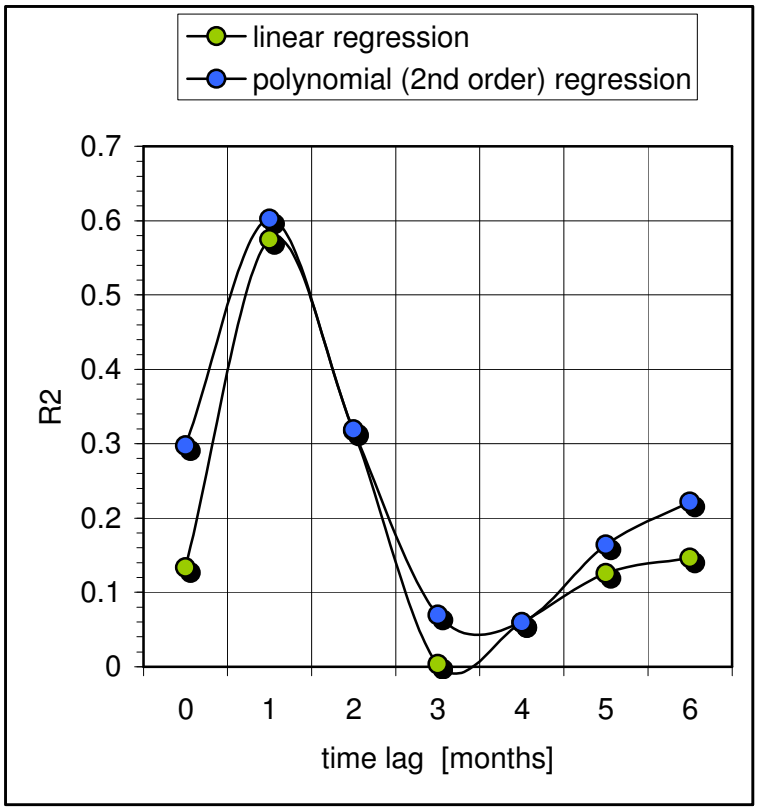

Plate 25. Plot of R^2 values derived from linear/polynomial (2^{nd} order) regressions of SeaWiFS-derived (JRC data set) *Chl* and GETM-derived mixed layer depth *(MLD)*, at successive time lags.

6. Conclusion

Algal growth in the Mediterranean Sea is always nutrient-limited, with consequent low biomass and primary production. The fertilization of the basin, supporting recurrent and sometimes anomalous algal blooming, is ruled mainly by the impact of (coastal interactions and) atmospheric forcing, and by the ensuing thermohaline processes. In the Ligurian-Provençal Sea, intense winter winds lead to convective processes that promote nutrient upwelling and then sustained spring blooms, once the wind regime relaxes and surface stratification sets in. The development of the classical sequence going from a period of deep convection – which generates the so called "blue hole" in the pigment field – to the following spring bloom, off the Gulf of Lion, represents one of the most distinct features among the environmental hotspot of the basin, as well as the main blooming event of the entire Mediterranean Sea, not driven directly by continental runoff.

The comparison of remote sensing data and model simulations, for the Gulf of Lion, shows that atmospheric forcing is the critical factor sustaining ecosystem dynamics in that area. Strong fall winds start to set up conditions favourable for algal growth, through vertical mixing and nutrient enrichment of surface waters. The biological response of the ecosystem is not instantaneous, after this set up, but fall blooming does recur in the later part of the year. As winter winds become even stronger, the continuing deep convection prevents the blooming to continue (and leads instead to the formation of a "blue hole"). Thus, stronger winds, above a certain threshold, are linked to stronger convection, but to lower pigment values in the surface layer. This increases nutrient concentration in the surface layer and generates conditions extremely favourable to algal growth, in late winter or early spring.

A prolongued period of convection delays the development of a (spring) bloom, but it also increased nutrient availability to the point that, once the water column stabilizes and stratification sets in, the blooming reaches unprecedented levels. Such a "delayed-mode" blooming, with a peak in April, is not uncommon, in the 1997-2007 decade (and, apparently, was so common as to appear in the historical climatological record of 1979-1985). But an "early-mode" blooming, with a peak in March, occurs just as often, during the same period. Given the relationship between prolongued convection and ensuing (late) blooming, it would be reasonable to assume that it is the wind regime of late fall, early winter to result critical in pre-conditioning the deep convection area, the entire Ligurian-Provençal Sea in fact, and in determining when the blooming will occur, and how intense it will be, in the following spring. However, no particular trends appear in the wind fields, or the physical structure of the mixed layer, in the periods preceding the "early mode" blooming. Hence, the hypothesis of global warming increasing the surface temperature of the Mediterranean

Sea, and therefore anticipating the onset of stratified condition, in certain years, could provide an explanation of the observed bloom anticipation. In fact, a stronger stratification would imply a lower rate of nutrient enrichment in the surface layer and a reduced *Chl* concentration (across the basin). It remains to be seen whether the winters preceding the "early-mode" blooming were particularly warm, or had other peculiar characteristics, so as to justify an anticipated onset of the stratification.

This study demonstrates that an improved interpretation of remote sensing data sets, and of the bio-geo-physical processes responsible for the observed phenomena, can be achieved through the combination of multi-sensor techniques and model simulations. However, it is obvious that knowledge of the variability of pigment concentrations, sea surface temperature, surface winds and mixed layer physical parameters is not sufficient for a full understanding of ecological dynamics in the environmental hotspot of interest. Improved modeling of the correlation between *Chl*, *SST*, *WS*, mixed layer physical parameters (*MLT*, *MLD*) and other environmental variables (*e.g.* primary production), planned for the future development of this line of work, might be able to provide more clues on the coupling between algal blooms and atmospheric forcing in the Mediterranean Sea. It should be noted, however, that much longer data sets would be required for a long-term analyses of the Mediterranean trends, particularly for the case of local changes in times of global warming.

References

Amante, C., and B.W. Eakins (2008). "*ETOPO1 1 Arc-Minute Global Relief Model: Procedures, Data Sources and Analysis*". National Geophysical Data Center, NESDIS, NOAA, U.S. Department of Commerce, Boulder, CO.

Antoine, D., ed. (2004). *Guide to the creation and use of ocean-colour, Level-3, binned data products.* IOCCG Report 4, pp. 88.

Backhaus, J.O., H. Wehde, E.N. Hegseth, and J. Kampf (1999). "Phyto-convection: the role of oceanic convection in primary production". *Marine Ecology-Progress Series*, vol. 189, p. 77-92.

Barale, V. (2000). "Integrated geographical and environmental remotely-sensed data on marginal and enclosed basins: the Mediterranean case". In: D. Wright and D. Bartlett ed.s, *Marine and Coastal Geographic Information Systems*, Taylor & Francis 'Research Monographs in Geographic Information Systems' series, London, p. 177-187.

Barale, V. (2003)."Environmental remote sensing of the Mediterranean Sea". *Journal of Environmental Science and Health*, vol. A3, no. 8, p. 1681-1688.

Barale, V. (2005). "Satellite observations as indicators of the health of the Mediterranean Sea", in: A. Saliot ed., *The Mediterranean Sea*, The Handbook of Environmental Chemistry, Volume 5 Water Pollution, Part K, Springer-Verlag Berlin, Heidelberg, p. 387-408.

Barale, V., J.M. Jaquet and M. Ndiaye (2008). "Algal blooming patterns and trends in the Mediterranean Sea as derived from the SeaWiFS data set (1998-2003). *Remote Sensing of Environment, special issue on: Earth Observations for Marine and Coastal Biodiversity and Ecosystems*, Vol. 112, No. 8, p. 3300-3313.

Bosc, E., Bricaud, A., and D. Antoine (2004). "Seasonal and interannual variability in algal biomass and primary production in the Mediterranean Sea, as derived from 4 years of SeaWiFS observations". *Global Biogeochemical Cycles*, 18, GB1005, doi:10.1029/2003GB002034.

Burchard, H., and K. Bolding (2002). "*GETM. A general estuarine transport model. Scientific documentation*". European Commission Publication, no. EUR 20253 EN, Ispra (Italy).

Cushing, D.H. (1959). "The seasonal variation in oceanic production as a problem in population dynamics". *Journal du Conseil, CIEM*

Conseil International pour l'Exploration de la Mer / ICES International Council for the Exploration of the Sea, vol. 24, no. 3, p. 455–464.

Donelan, M.A., and W.J. Pierson (1987). "Radar scattering and equilibrium ranges in wind-generated waves with application to scatterometry", *Journal of Geophysical Research*, vol. 92, p. 4971-5029.

Draper, D.W, and D.G. Long (2002). An assessment of SeaWinds on QuikScat wind retrieval. *Journal of Geophysical Research*, 107 (C12), 3212, doi:10.1029/2002JC001330.

Gregg, W.W., and N.W. Casey (2004). Global and regional evaluation of the SeaWiFS chlorophyll data set. *Remote Sensing of Environment*, vol. 93 (4), p. 463-479.

Hermann, M., S. Somot, F. Sevault, C. Estournel, and M. Déqué (2008). "Modeling the deep convection in the northwestern Mediterranean Sea using an eddy-permitting and an eddy-resolving model: case study of winter 1986-87". Journal of Geophysical Research, vol. 113, C04011, doi:10.1029/ 2006JC003991.

Hovis, W.A., D.K. Clark, F. Anderson, R.W. Austin, W.H. Wilson, E.T. Baker, D. Ball, H.R. Gordon, J.L. Mueller, S.Z. El-Sayed, B. Sturm, R.C. Wrigley, and C.S. Yentsch (1980). "Nimbus-7 Coastal Zone Color Scanner system description and initial imagery". *Science,* vol. 210, p. 60-63.

International Hydrographic Organization (1953). *Limits of Oceans and Seas*. Special Publication No. 23, 3rd Edition, Imp. Monégasque, Monte Carlo, pp. 39.

Kidwell, K.B. (1991). *NOAA polar orbiter data users guide.* National Environmental Satellite and Data Information Service, U.S. Governamental Printing Office, Washington DC, USA.

Kilpatrick, K.A., G.P. Podesta and R. Evans (2001). Overview of the NOAA/NASA Advanced Very High Resolution Radiometer Pathfinder algorithm for sea surface temperature and associated matchup database. *Journal of Geophysical Research*, *Oceans*, 106 (C5): 9179-9197.

Kondrachoff, V., C. Estournel, P. Marsaleix, R. Vehil, and R.M. Zbinden (1994). "Detection of the Rhone River plume using NOAA-AVHRR data – comparison with hydrodynamic modelling results". In: J.A. Johannessen and T.H. Guymer eds., *Oceanic*

Remote Sensing and Sea Ice Monitoring, Proceedings SPIE Vol. 2319, p. 73-84.

Looser, U., I. Dornblut, and T. de Couet (2007). The Global Terrestrial Network for River Discharge (GTN-R): Real-time Access to River Discharge Data on a Global Scale. 1st Interim Report / GRDC Report 36, pp. 24 (annex pp. 42).

Maillard, C., M. Fichaut, G. Maudire, C. Coatanoan, E. Balopoulos, A. Iona, A. Lykiardopoulos, P. Karagevrekis, J.-M. Beckers, M. Rixen, M.-J. Garcia, B. Manca, A. Giorgetti, A. Mosetti, N. Mikhailov, E. Vyazilov, A. Kuznetsov, N. Puzova, R. Boukortt, B. Boudjellal, N. Eddalia, H. Dooley, A. Drago, S. El-Agami, G. Kortchev, I. Gertman, Y. Tsehtik, S. Lakkis, G. Manzella, I. Oliounine, A. Orbi, J. Larissi, S. Zizah, M. Ozyalvac, F. Berkay, N. Pinardi, M. Zavatarelli, A. Suvorov, A. Khaliulin, G. Zodiatis, K. Bilashvili, Z. Savaneli, V. Dadic, V. Diaconu, R. Gelfeld, and C. Sammari (2005). "A Mediterranean and Black Sea Oceanographic Database and Network". *Bollettino di Geofisica Teorica ed Applicata,* vol. 46, n. 4. p. 329-343.

Mann, K. H., and Lazier, J.R.N. (2006). *Dynamics of Marine Ecosystems: Biological-Physical Interactions in the Oceans.* Third edition. Blackwell Publishing, Malden, MS, pp. 496.

McClain, C.R., G.C. Feldman, and S.B. Hooker (2004). "An overview of the SeaWiFS project and strategies for producing a climate research quality global ocean bio-optical time series". *Deep-Sea Research,* vol. II 51, p. 5-42.

Millot, C., and I. Taupier-Letage (2005), "Circulation in the Mediterranean Sea", in: A. Saliot ed., *The Mediterranean Sea*, The Handbook of Environmental Chemistry, Volume 5 Water Pollution, Part K, Springer-Verlag Berlin, Heidelberg, p. 31-66.

Murray, M.J., M.R. Allen, C.T. Mutlow, A.M. Zavody, T.S. Jones, and T.N. Forrester (1998). "Actual and Potential Information in Dual-View Radiometric Observations of Sea Surface Temperature from ATSR". *Journal of Geophysical Research*, vol. 103, p. 8153-8165.

Nykjaer, L. (2008). "Mediterranean Sea surface warming from 1985 to 2006". *Climate Research*, in press.

Petrenko, A., Y. Leredde, and P. Marsaleix (2005). "Circulation in a stratified and wind-forced Gulf of Lion, NW Mediterranean Sea: in situ and modeling data". *Continental Shelf Research*, vol. 25, p. 7-27.

Rodwell, M.J., D.P. Rowell, and C.K. Folland (1999). “Oceanic forcing of the wintertime North Atlantic oscillation and European climate”. *Nature*, no. 398, pp. 320-323.

Sathyendranath, S., ed. (2000). “*Remote Sensing of Ocean Colour in Coastal, and Other Optically-Complex, Waters*”. IOCCG Report 3, pp. 140.

Schott, F., M. Visbeck, U. Send, J. Fisher, L. Stramma, and Y. Desaubies (1996). “Observations of deep convection in the Gulf of Lion, Northern Mediterranean, during the winter of 1991/92”. *Journal of Physical Oceanography*, vol. 26, p. 505-524.

Schroeder, L.C., D.H. Boggs, G. Dome, I.M. Halberstam, W.L. Jones, W.J. Pierson, and F.J. Wentz (1982). “The relationship between wind vector and normalized radar cross section used to derive Seasat-A satellite scatterometer winds”. *Journal of Geophysical Research,* vol. 87, p. 3318-3336.

Stips, A., H. Burchard, K. Bolding, and W. Eifler (2002). “Modelling of convective turbulence with a two-equation k-ε turbulence closure scheme”. Ocean Dynamics, vol. 52, p. 153-168.

Yoder, J.A., and M.A. Kennelly (2003). “Seasonal and ENSO variability in global ocean phytoplankton chlorophyll derived from 4 years of SeaWiFS measurements”. Global Biogeochemical Cycles, vol. 17, no. 4, p. 1112-1126.

Zavody, A.M., C.T. Mutlow and D.T. Llewellyn-Jones (1995). “A Radiative Transfer Scheme for SST Retrieval for the ATSR”. *Journal of Geophysical Research*, vol. 100, p. 937-952.

European Commission

EUR 23708 EN – Joint Research Centre – Institute for Environment and Sustainability
Title: Near-Coastal Features of the NW Mediterranean Sea. Space and time heterogeneity of atmospheric forcing, vertical mixing and algal blooming, from satellite observations and model simulations (1997-2007).
Authors: V. Barale, E. Garcia Gorriz, n. Hoepffner, A. Stips
Luxembourg: Office for Official Publications of the European Communities
2008 – 60 pp. – 21.0 x 29.7 cm
EUR – Scientific and Technical Research series – ISSN 1018-5593

Abstract

Data derived from satellite observations and model simulations were used to assess space–time heterogeneity of atmospheric forcing, vertical mixing and algal blooming of the Ligurian-Provençal Sea, in the north-western Mediterranean basin. The ecosystem response to changing seasonal conditions in the Gulf of Lion (40.5–42.5°N, 3.5–7.5°E) was examined over 10 consecutive annual cycles (September 1997 – August 2007). In this environmental hotspot, atmospheric forcing causes deep convective processes and consequent nutrient upwelling in the water column. As phytoplankton growth in the otherwise oligotrophic basin is always nutrient-limited, the blooming triggered by these processes reflects the prevailing wind field patterns.

How to obtain EU publications

Our priced publications are available from EU Bookshop (http://bookshop.europa.eu), where you can place an order with the sales agent of your choice.

The Publications Office has a worldwide network of sales agents. You can obtain their contact details by sending a fax to (352) 29 29-42758.

The mission of the JRC is to provide customer-driven scientific and technical support for the conception, development, implementation and monitoring of EU policies. As a service of the European Commission, the JRC functions as a reference centre of science and technology for the Union. Close to the policy-making process, it serves the common interest of the Member States, while being independent of special interests, whether private or national.